Evolutionary origins and transcriptomic innovations of vertebrate Cajal-Retzius cells

Elias Gumnit[1], Giacomo Gattoni[1], Jamie Woych[1], Astrid Deryckere[1#], Prabesh Bhattarai[2,3], J Andrew Gillis[4], Caghan Kizil[2,3], Maria Antonietta Tosches[1*]

[1] Department of Biological Sciences, Columbia University, New York, NY, USA.
[2] Department of Neurology, Columbia University Irving Medical Center, New York, NY, USA
[3] The Taub Institute for Research on Alzheimer's Disease and the Aging Brain, Columbia University Irving Medical Center, New York, NY, USA
[4] Bay Paul Centre, Marine Biological Laboratory, Woods Hole, MA, USA

[#] Present address: Laboratory of Reproductive Genomics, KU Leuven, Leuven, Belgium

* Corresponding author. Email: mt3353@columbia.edu

Abstract

Evolutionary changes of cortical development were instrumental for the emergence of the mammalian neocortex. Cajal-Retzius cells, a transient neuron type discovered over a century ago, are critical players in the development of mammalian-specific cortical features such as inside-out corticogenesis. However, it is unclear whether Cajal-Retzius cells exist only in mammals, or if they are ancestral in vertebrates but acquired new functions during mammalian brain development. To trace the evolution of this cell type, we probe the presence of Cajal-Retzius cells in chicken, salamander, zebrafish, and little skate. First, through comparative transcriptomics and spatial analysis we show that Cajal-Retzius cells are conserved in vertebrates. However, only amniote Cajal-Retzius cells gained robust expression of *Reelin*, a secreted glycoprotein crucial for mammalian cortical development. Second, we find that Cajal-Retzius cells are part of a larger and diverse family of neuron types, and are closely related to *Tp73*+ external tufted cells in the olfactory bulb, which express most of the "canonical" Cajal-Retzius transcription factors. Our results indicate that Cajal-Retzius cells emerged early in vertebrate history, using a regulatory program largely shared with neurons in the olfactory system, and that transcriptomic novelties underlie their specialized roles in mammalian cortical development. This is an extreme example of how cell types may diverge in morphology and function over the course of evolution even when their core transcriptomic profile is broadly preserved.

Introduction

The forebrain is the brain region that underwent the most dramatic changes in vertebrate evolution [1]. In mammalian ancestors, the drastic expansion of the pallium (dorsal telencephalon) occurred with several innovations, including the anatomical and

functional diversification of cortical regions, a six-layered neocortex, and a folded hippocampus. Changes in cortical development may underlie the evolution of these novelties [1,2]. To investigate the underpinnings of these changes, we focused on Cajal-Retzius (CR) cells, a multifunctional cell type with critical roles in the development of mammalian-specific cortical traits [3–6]. In mammals, CR cells are born in the ventral pallium, cortical hem, septum, and prethalamic eminence (PThE), and then migrate tangentially in the marginal zone to cover the entire telencephalic vesicle [7–12]. These cells are the major source of Reelin, a secreted molecule that regulates the radial migration of immature neurons during corticogenesis [13,14]. CR cells also control cortical arealization, serve as pioneer neurons in the hippocampus and olfactory system, influence hippocampal morphogenesis, and regulate circuit assembly in the hippocampus and neocortex [8,14–25]. Clarifying the evolution of CR cells is thus essential to understand how innovations in the mammalian cerebral cortex emerged.

Notably, while CR cells are the first neurons that develop in the mammalian pallium, their evolution remains highly debated. Markers of mammalian CR cells, including Reelin and the transcription factor p73, are expressed in scattered pallial cells in developing lizard, crocodile, chicken, frog, and fish brains [26–30]. A recent study proposed that CR cells existed already in tetrapod ancestors [30], but the interpretation of chick data is contentious [29,31,32], and fishes remain poorly investigated. The expression of single CR markers remains insufficient to conclude whether CR cells exist in non-mammals: none of these markers are CR-specific, but it is only their *combined* expression that defines CR identity[3].

With the advent of single-cell RNA sequencing, mammalian CR cells have been well characterized at the transcriptomic level, and express a core set of transcription factors (TFs) including: *Tp73, Tbr1, Lhx1, Lhx5, Ebf2, Ebf3, Nr2f2, Nhlh2,* and *Barhl2* (with *Tp73* and *Ebf3* missing in ventral-pallium derived cells) [5,33]. Among these, *Tp73* (*Trp73* in mice) encodes for p73 and is expressed in CR cells derived from medial sources (PThE, septum, and hem). (For simplicity, hereafter we refer to the mouse *Trp73* gene as *Tp73*). *Tp73* is a key player in the gene regulatory network that establishes medial CR identity: mutant mice display abnormal cortical lamination and hippocampal malformations in conjunction with loss of medial CR cells [26,29].

Here we explored the evolution of CR cells by examining species that represent the main branches of the vertebrate tree. Expanding on previous work[27–30,34], we found *Tp73*+ cells in the pallium and other conserved spatial locations in all vertebrate species examined. Motivated by these observations, we then performed unbiased transcriptomic comparisons to identify CR-like neurons in non-mammalian species. In-depth analyses revealed that *Tp73* defines a diverse and evolutionarily-conserved family of neurons, including not only CR cells, but also neurons in the olfactory bulb (OB) and in the basal forebrain. With our cross-species analyses, we identify the conserved set of transcription factors that differentiate CR cells from their closely-related neuron types, and identify critical evolutionary innovations of the CR cell transcriptome. Taken together, our findings indicate that CR cells were already present in vertebrate ancestors and share evolutionary origins with a neuron type in the OB, raising new scenarios on the early evolution of this enigmatic cell type.

Results

Conserved populations of *Tp73*+ neurons in vertebrates

In the developing mouse brain, *Tp73* is expressed in neurons distributed within the pallium, subpallium, olfactory bulb (OB), preoptic area (POA), and prethalamic eminence (PThE, a diencephalic region that persists after development only in amphibians and fish)[35]. *Tp73* is expressed also in some non-neuronal cells including the choroid plexus, which develops from the cortical hem (Fig. 1A) [36]. Pallial *Tp73*+ neurons are CR cells and express *Reln*, whereas diencephalic *Tp73*+ neurons that do not coexpress *Reln* are not classified as CR cells [35,37] (Fig. 1A).

Using HCR *in situ* hybridization, we characterized the distribution of *Tp73*+ neurons during brain development in multiple species representing the major vertebrate clades. Scattered *Tp73*+ neurons have been reported in the developing chick brain [29]. These *Tp73*+ neurons are most dense near the cortical hem and grow sparser laterally into the medial and dorsal pallium (Fig. 1B). We also observed *Tp73*+ neurons in the chick subpallium, PThE, and OB (Fig. 1B, fig. S1A). Overall, the distribution pattern was similar to the one previously observed in lizard embryos, where *Tp73*+ neurons were found in the PThE, subpallium, and OB, plus sparse *Tp73*+ neurons in the pallium [27] (Fig. 1A). In the salamander *Pleurodeles waltl,* we found scattered *Tp73*+ neurons also distributed throughout the pallium - with higher density around the hem - from early to late stages of pallial neurogenesis [38]. In addition, *Tp73*+ cells were visible in the OB, PThE, and subpallium (Fig. 1C, fig. S1B, video S1).

We then extended our analysis to two distantly-related fish species: the teleost zebrafish and a cartilaginous fish, the little skate *Leucoraja erinacea*. In the developing zebrafish forebrain, *tp73*+ cells were present in the same brain regions described in tetrapods, with sparse *tp73*+ neurons in the pallium (Fig. 1D, fig S1C, video S2). In the developing skate, *Tp73*+ neurons were found in high density in the OB and pallium, and more sparsely in the subpallium and putative PThE, consistent with other vertebrates (Fig. 1E, fig. S1D).

In the adult mouse brain, *Tp73*+ neurons persist in the OB, basal forebrain, and pallium, although only a small percentage of CR cells in the pallium survives to adulthood [39]. Consistently, we found *Tp73*+ neurons in the same brain areas, plus the PThE, in adult salamander, zebrafish, little skate, and in the bichir fish *Polypterus senegalus* (a non-teleost ray-finned fish), but with a drastic reduction of the density of *Tp73*+ pallial cells, particularly in skates (fig. S2, video S3-4). These results indicate that the spatial pattern of *Tp73* expression is conserved across jawed vertebrates, with at least some *Tp73* neurons in the developing pallium, where in mammals *Tp73* is highly specific to CR cells born from medial sources (cortical hem, septum, and PThE).

Motivated by these observations, we asked whether neurons resembling mammalian CR cells at the transcriptome level exist in the developing forebrain of non-mammalian species. For this we relied on our recent high quality scRNA-seq dataset of the developing salamander brain[40], which spans eight developmental stages and multiple brain regions. Only one cluster in this dataset expressed high levels of *Tp73* (Fig. 2A-B). This cluster also expressed neuronal markers, such as the synaptic gene *Snap25* and the vesicular glutamate transporter gene *Slc17a6*, which clearly differentiated it from non-neuronal cells expressing low levels of *Tp73* (fig. S3B).

132 Importantly, TFs usually associated with mammalian CR cells, including *Tp73*, *Lhx1*,
133 *Lhx5*, *Nr2f2*, *Ebf2*, *Ebf3*, and *Barhl2* [5], were co-expressed only in the *Tp73*+ neuronal
134 cluster (Fig. 2B, fig. S3A). To further determine whether these salamander *Tp73*+
135 neurons are the most similar to mouse CR cells at the transcriptomic level, we
136 compared our scRNAseq data with a developmental mouse brain dataset [41], restricting
137 our analysis to mature neurons (see Methods). We used three independent methods to
138 compare the salamander and mouse datasets. First, we computed all the genes that
139 differentiate mouse CR cells from other mouse differentiated neurons, and then
140 assessed the relative expression enrichment for these genes in the salamander dataset.
141 *Tp73* neurons in salamander showed the highest enrichment for this CR gene module
142 (Fig. 2C). Second, we computed pairwise transcriptomic correlations (gene specificity
143 index [42], see Methods) of all salamander and mouse neuron classes, and found that the
144 salamander *Tp73*+ neurons are most similar to mouse CR cells (Fig. 2D). Third, using
145 manifold integration [43] for the joint analysis of the two data sets, we identified a cluster
146 in the integrated transcriptomic space that includes salamander *Tp73*+ neurons and
147 mouse CR cells, supporting the transcriptomic similarity of these cell types (Fig. 2E, fig.
148 S4A-D). These data suggest a close transcriptomic similarity of salamander *Tp73*+
149 neurons and mouse CR cells.
150 Next, we analyzed transcriptomic data from zebrafish to assess the existence of
151 neurons similar to salamander *Tp73*+ neurons. In a dataset by Pandey et al. [44] from the
152 developing zebrafish forebrain, a glutamatergic cell type annotated as "olfactory bulb"
153 (OB) expressed many of the TFs characterizing mammalian CR cells and salamander
154 *Tp73*+ neurons such as *lhx1a*, *lhx5*, *ebf3*, and *barhl2* (Fig. 2F-G, fig. S5A-F). *tp73* was
155 poorly detected in this dataset, probably due to technical reasons; supporting this
156 conclusion, this gene was detected in a more deeply-sequenced adult dataset [45], where
157 it was coexpressed with other CR TFs (see fig. S5L-S). The OB cluster also showed the
158 highest enrichment score for genes that distinguish *Tp73*+ neurons from other neuron
159 types (Fig. 2H). GSI correlation analysis of zebrafish and salamander neurons showed
160 a significant correlation between salamander *Tp73*+ neurons and the zebrafish OB
161 cluster. (Fig. 2I). In addition, integration of salamander and zebrafish data showed co-
162 clustering of zebrafish OB cells and a subset of salamander *Tp73*+ neurons; a second
163 group of salamander *Tp73*+ neurons co-clustered with zebrafish diencephalic neurons,
164 suggesting transcriptomic heterogeneity (Fig. 2J, fig. S4E-H). We conclude that the
165 zebrafish OB cluster has high similarity to salamander *Tp73*+ neurons (markers of OB
166 mitral cells, the major OB glutamatergic type, are expressed in a separate set of cells,
167 see fig. S5H-K). Taken together, these results indicate that *Tp73*+ neurons are overall
168 highly similar at the transcriptomic level in mouse, salamander, and zebrafish,
169 supporting their evolutionary conservation in vertebrates.
170
171 **Heterogeneity of salamander *Tp73*+ neurons**
172 The presence of *Tp73*+ cells in different areas of the forebrain (Fig. 1), together
173 with the varied expression of marker genes in *Tp73*+ neurons (Fig. 2) suggests they are
174 heterogeneous. Therefore, we sought to further characterize the molecular
175 heterogeneity of salamander *Tp73*+ neurons in order to clarify their comparison with
176 mammalian CR cells. To increase the power of our analyses, we merged *Tp73*+
177 clusters from larval and adult [46] scRNA-seq datasets, after noticing that *Tp73*+ neurons

have conserved transcriptomes and spatial distribution across the salamander lifespan (fig. S2A-B). This salamander *Tp73*+ dataset, restricted to neurons, contained 982 cells (Fig. 3A, fig. S6).

After clustering and differential gene expression analysis, we identified three major classes of *Tp73*+ neurons, each including multiple clusters. The first class comprised late progenitors and immature neurons, as indicated by the expression of the proliferation marker *Mki67*, low levels of the synaptic gene *Snap25*, and markers of immature neurons like *Vim* and *Neurod4* (clusters im1-2, Fig. 3A-B). These clusters were uniquely labeled by *Gmnc* and *Cccno*, members of a multiciliation gene module expressed transiently during early CR differentiation in mice [29]. Double HCR *in situ* hybridization showed coexpression of *Tp73* with *Gmnc* and *Ccno* in sparse cells in the hem, septum, and PThE (fig. S7). These observations suggest that cells in clusters im1-2 are in the process of acquiring a terminal CR-like neuronal fate.

The other two classes were identified as mature *Tp73*+ neurons. The first class (clusters m1.1 to 1.4) shared some of the defining features of CR cells, including *Ebf2* and *Ebf3* expression and absence of *Foxg1* expression. The second class (clusters m2.1 to m2.8) expressed the unique combination of *Stk32a*, *Elfn1*, and *Sorcs1* (Fig. 3B). We performed HCRs to locate these two distinct populations in the developing brain. *Stk32a* and *Tp73* (m2 class) were coexpressed in the subpallium and PThE, but not in the OB or pallium. In contrast, *Ebf3* and *Tp73* (m1 class) were coexpressed in cells in the OB and pallium, but not in the subpallium or PThE (Fig. 3C, fig. S8A-B). We conclude that mature salamander *Tp73*+ neurons belong to spatially and molecularly distinct populations: a population of *Tp73*+ *Ebf3*+ neurons enriched in the anterior and dorsal forebrain, and a second population of *Tp73*+ *Ebf3*- neurons in the posterior and ventral forebrain. These two neuronal classes co-cluster with different sets of neurons in the zebrafish dataset, suggesting an ancient origin (fig. S8C).

Next, we explored further the heterogeneity of *Tp73*+ *Ebf3*+ neurons. Cluster m1.1 expressed high levels of *Nfix* and *Nfia*, markers of mammalian hem-derived CR cells [33]. When staining for *Nfix*, we found coexpression with *Tp73* only in the pallium, including the hem region, and not in the OB (Fig. 3D, fig S8D-E). Conversely, clusters m1.2-4 expressed *Asic4* and *Cdhr1*, markers of mammalian OB glutamatergic neurons [47,48]. *Asic4* showed the opposite pattern as *Nfix*, as it was coexpressed with *Tp73* in OB but not in pallium (Fig. 3D, fig S8D). This suggests that the *Tp73*+ *Ebf3*+ class of salamander neurons includes a pallial population with additional markers of mammalian CR identity, and an OB population expressing markers of OB glutamatergic neurons.

Cajal-Retzius and olfactory bulb *Tp73*+ external tufted cells are sister cell types

Next, we investigated whether the molecular and spatial heterogeneity of salamander *Tp73*+ neurons has counterparts in mammals. We isolated mouse *Tp73*+ neurons from the Allen Brain Cell (ABC) atlas [39] and compared them to the salamander *Tp73*+ neuron dataset. The ABC atlas, comprising the entire adult mouse brain, was chosen for its high sequencing depth, completeness, and matching MERFISH data, necessary to resolve subtle differences between *Tp73*+ neurons types. This atlas includes three populations of *Tp73*+ neurons (Fig. 4A and fig. S9A-B). One is composed of subclass 118 ADP-MPO Trp73 and cluster 2111 LHA Barhl2 Glut_2, spatially located in the basal forebrain, specifically in areas annotated as the lateral hypothalamus and

medial POA. A second group is the subclass 036 HPF CR Glut, which includes CR cells sampled from the adult cortex and hippocampus (Fig. 4A, fig. S9A). Finally, a third group is the supertype 0132 OB Eomes Ms4a15 Glut_3, which was further characterized by Zeppilli et al [47] in a transcriptomic analysis of the OB. These cells express *Lhx1* and *Ebf3* and correspond to one type of external tufted cells (ETCs) (see cluster ET2 in Zeppilli et al [47]). ETCs are a heterogeneous class of glutamatergic neurons in the mammalian OB; these cells, or at least a subset of them, are believed to be born in the pallium before migrating to the bulb [49–51]. The *Tp73*+ ETCs are juxtaglomerular tufted cells that synapse with olfactory sensory neurons and other periglomerular interneurons [52,53] (fig. S10). Using cross-species data integration, we found that classes of salamander *Tp73*+ neurons integrate with distinct mouse *Tp73*+ neurons. We computed the overlap of cells' cross-species neighborhoods in the integrated transcriptomic space (see Methods). Salamander *Tp73*+ *Ebf3*- neurons were on average more similar to mouse basal forebrain *Tp73*+ neurons, while salamander *Tp73*+ *Ebf3*+ neurons were more similar to mouse CR and ETC (Fig. 4C). Specifically, salamander clusters m1.1 (*Nfix*+) and m1.2 were most likely to be mutual nearest neighbors with mouse CR cells (Fig. 4C) and also co-clustered with them (fig. S11A-C), while m1.4 (*Asic4*+) neurons were nearest neighbors with mouse ETC cells in the integrated space (Fig. 4C) and co-clustered together (fig.S11A-C). GSI correlation analysis showed a similar trend, although this analysis was less sensitive than integration at distinguishing CR and ETC cells due to the high transcriptomic similarity between these two cell types (Fig. 4D). These comparisons indicate that salamander *Tp73*+ *Ebf3*+ *Nfix*+ neurons are homologous to mammalian CR cells, while salamander *Tp73*+ *Ebf3*+ *Asic4*+ neurons are homologous to ETCs.

Next, we wondered whether transcriptomically distinct CR and ETC cells exist in other vertebrate species. The available chicken [54] and zebrafish [44] datasets had several limitations, including low numbers of *Tp73*+ neurons, absence of OB sampling (in chicken), and relatively lower sequencing depth (in zebrafish). Nevertheless, comparisons of chicken and zebrafish *Tp73*+ neurons with mouse ABC Atlas *Tp73*+ neurons supported the conclusion that the chicken *Tp73*+ neurons in Zaremba et al. [54] are CR cells (fig. S10, fig. S11D-F), and that most zebrafish *tp73*+ neurons in Pandey et al. [44] are ETCs (fig. S11G-I). The fact that a few zebrafish cells co-clustered with mouse CR cells (fig. S11G-I), together with our tissue staining data (Fig. 1), is consistent with the possibility that CR cells also exist in teleosts.

To further support the existence of *Tp73*+ ETCs across vertebrates, we analyzed *Tp73* expression in the mature OB, where glomeruli are well defined. The mouse *Tp73*+ ETCs have a characteristic spatial distribution: they surround the olfactory glomeruli [47] (Fig. 4G). We observed *Tp73*+ neurons in the glomerular layer of salamander, bichir, zebrafish, and skate (Fig. 4G). In the three fish species, *Tp73* neurons were arranged in characteristic rings around the glomeruli (Fig. 4G). These results indicate that *Tp73*+ ETCs are a conserved neuron type in jawed vertebrates.

Finally, we asked whether the expression of similar sets of transcription factors underlies the transcriptomic similarity of CR cells and ETCs. A comparison of TFs expressed in mouse CR and ETC cells but not in other OB glutamatergic neurons (see Methods) showed that mouse CR and ETC cells expressed different sets of TFs overall, but shared the expression of many TFs usually associated to CR identity (fig. S9D). Of

these, *Nr2f2*, *Tp73*, *Dach1*, *Ebf3*, *Zeb2*, *Lhx1*, *Nr2f1*, *Tbr1*, *Id4* and *Hivep1* were expressed also in chicken CR cells and in salamander CR and ETCs (zebrafish ETCs lacked *Nr2f2*, *Tp73*, *Zeb2* and *Hivep1* expression, but we cannot rule out technical limitations) (Fig. 5A). These results indicate that, at least in tetrapods, many "canonical" CR transcription factors are also expressed in ETCs.

Therefore, we asked whether the molecular identities of ETC and CR cells are defined by the expression of different sets of TFs, *i.e.* if these two cell types are genetically individuated [55]. Specifically, we looked for TFs that could consistently discriminate between ETC and CR cell identities across vertebrates. First, we identified TFs that had conserved differential expression between ETC and CR cells in both salamander and mouse, and then assessed their expression in chicken CRs and zebrafish ETCs (see Methods). While we couldn't find any conserved ETC-specific TFs, we observed that *Zic1*, *Zic2*, and NFI-family TFs were expressed in CR but not in ETCs in mouse and salamander, and that these TFs were expressed in chicken CRs too but not in zebrafish ETCs (Fig. 5B). Notably, in mouse NFI-family TFs are specific to hem-derived CR cells [33], suggesting that the CR cells sampled in salamander and chicken are mostly hem-derived, in line with our HCR data.

Finally, we checked for the presence of these CR-specific TFs in skate *Tp73*+ neurons (Fig. 5C). *Tp73* neurons in the subpallium expressed *Zic1* but not *Nfia*. Moreover, the *Tp73*+ cells in the OB did not express *Nfia* or *Zic1*, consistent with ETC identity. However, *Tp73* showed co-expression with both *Nfia* and *Zic1* in the skate pallium, indicating that these are CR cells. These combinations of markers in the little skate suggest that the major classes of *Tp73*+ neurons existed in the last common ancestor of jawed vertebrates.

Taken together, the high degree of transcriptome and TFs expression similarity of ETC and CR cells suggests that these cell types have a shared evolutionary origin. Across different vertebrate species, CR cells could be consistently distinguished from ETCs for the expression of *Zic* and NFI transcription factors, suggesting that these TFs were recruited in ancestral vertebrates to differentiate the identities of these two cell types.

Transcriptomic divergence of vertebrate Cajal-Retzius cells

The presence of CR cells in non-mammals challenges the notion that mammalian-specific cortical traits emerged with the appearance of this cell type in evolution. Alternatively, CR cells might be a conserved cell type with diverging characteristics across species.

Since a key effector of mammalian CR function is the secreted protein Reln, we first asked whether the coexpression of *Tp73* and *Reln* is conserved across vertebrate species. In the developing chick brain, we found robust overlap of *Tp73* and *Reln* in the pallium and hem, corroborating scRNA-seq data (Fig. 6A, fig. S6H). However, stainings for *Tp73* and *Reln* in salamander revealed coexpression only in rare *Tp73* pallial neurons, consistent with scRNA-seq (fig. S7H). Furthermore, there was no coexpression of *Tp73* and *Reln* in the pallium of developing skates and zebrafish. This is most striking in the developing skate brain, where *Reln* is clearly absent from the dense layer of *Tp73* neurons at the pallial surface, but is expressed robustly elsewhere, including a separate population of pallial neurons (Fig. 6A, fig. S12). This suggests that

316 strong coexpression of *Tp73* and *Reln* may be an amniote innovation, in line with
317 observations in other species [28], and that *Reln* is not a conserved marker of CR cells
318 across all vertebrates.
319 To identify other species-specific specializations, we searched genes with
320 conserved and species-enriched expression in salamander and mouse CR cells. We
321 computed in each species the differentially expressed genes between CR cells and
322 other glutamatergic neurons in the developing pallium (developing mouse data from
323 Moreau et al. [29,33]); salamander CR cells were defined here as the mature neurons that
324 integrate with mouse CR cells (Fig. 4) and ETCs were excluded (see Methods). As
325 expected, the top shared markers included *Tp73*, *Ebf3, Zic1, Zic2* and other TFs (Fig.
326 6B). In addition, we found that the glutamate transporter *Slc17a6* (*Vglut2*), the
327 glutamate receptor *Grm2*, and general markers of immature neurons (*Msi1*, *Sox9*, *Vim*)
328 in CR cells from both species. *Cxcr4* and *Zic2*, essential for the proper migration and
329 positioning of CR cells in mice [56,57], were also expressed in salamander CR cells,
330 suggesting the evolutionary conservation of molecular mechanisms of CR migration.
331 The Netrin receptor *Unc5b* was also expressed in both salamander and mouse CR
332 cells. Importantly, *Nectin-1* (encoded by *Pvrl1*), *N-cadherin* (*Cdh2*) and *Mllt4* (*Afdn*)
333 were also expressed in CR from both species (fig. S13); in mouse, these adhesion
334 molecules are crucial for the interaction between CR cells and cortical neurons during
335 radial migration [58].
336 Interestingly, salamander and mouse CR cells expressed different sets of
337 synaptic genes, with *Lgi2, Erbb4, Rpha3, Zdhhc22*, and *St8s1a4* enriched in
338 salamander, and *Cacna2d2*, *Baiap2*, *S100a10*, and *Cpne2* enriched in mouse (Fig. 6B).
339 This divergent use of synaptogenesis genes may be due to differences in wiring
340 specificity, genetic drift, relative differences in maturation state[59] , or some other
341 species-specific adaptation. Furthermore, salamander and mouse CR cells differed in
342 the expression of neurotrophic, cell cycle, and apoptotic genes, with *Ngfr*, *Serpinf1*, and
343 *Erbb4* enriched in salamander, and *Cdkna1a* (p21), *Phlda3*, and *Tnfaip8* enriched in
344 mouse (Fig. 6B), suggesting diverging mechanisms for the regulation of neuronal
345 survival. Notably, the transcription factor *Dmrta2* was expressed in mouse but not
346 salamander CR cells (see also Fig. 4G). *Dmrta2* knock-out mice have significantly
347 reduced CR abundance [60], suggesting that gain of *Dmrta2* expression in amniote CR
348 cells may have contributed to their higher number and density.
349 Finally, we reasoned that if CR cells have some role during pallial development
350 also in non-mammals, their density should be highest during neurogenesis. This is
351 clearly the case in the little skate (compare Fig. 1E and fig. S2). After counting *Tp73*+
352 neurons in the salamander medial and dorsal pallium, which are mostly CR cells, we
353 saw that their density peaks during early pallial neurogenesis [38,40] (stage 46, with ~9000
354 cells per mm^3), and gradually decreases later (Fig. 6C). Taken together, our data
355 indicate that non-mammalian CR cells may be involved in early pallial development, but
356 use a divergent set of molecular effectors including Reln.

357 Discussion

358 Our molecular comparisons in fish, amphibians, birds, and mammals indicate
359 that *Tp73*+ Cajal-Retzius cells are an ancient cell type in vertebrates. These results
360 place CR cells as part of the broader family of *Tp73*+ neuron types. We identify two

conserved classes of *Tp73*+ neurons in vertebrates, with distinct transcriptomes and spatial distribution. A first class (*Tp73*+ *Ebf3*- cells) comprises cells in the PThE and basal forebrain. The PThE is the developmental source of several types of glutamatergic neurons that then migrate to other brain regions, including the preoptic area and hypothalamus [9,61,62]. We suggest that the *Tp73*+ *Ebf3*- cells we identified in salamander and zebrafish include the PThE and cells that have migrated to the basal forebrain. A second conserved neuronal class is defined by the coexpression of *Tp73* and *Ebf3*; these neurons are located in the olfactory bulb and in the pallium, particularly in the hem region. Further transcriptomic analyses indicate that these cells belong to two distinct types, the *Tp73*+ external tufted cells and the *Tp73*+ Cajal-Retzius cells. Our results, establishing that CR cells existed at least in the last common ancestor of jawed vertebrates, are largely in line with a recent scRNAseq study reporting CR cells in the shark *Scyliorhinus canicula* [63].

In mammals, CR cells originate from multiple forebrain regions, and *Tp73* is expressed in all subtypes except the ventral-pallium derived CR cells. Interestingly, all the CR cells we identified in scRNAseq datasets from non-mammalian species express markers of mammalian hem-derived CR cells such as NFI transcription factors. Although the hem might be the most prominent source of CR cells outside mammals, we cannot exclude the existence of septum and PThE-derived CR cells in non-mammals, as suggested by staining data for *Ccno* and *Gmnc* in salamander (fig. S7). The evolution of ventral-pallium derived CR cells, which do not express *Tp73*, remains unresolved. In our cross-species comparisons, only *Tp73*+ neurons had high transcriptomic similarity to mouse CR cells, but it is still possible that *Tp73*-negative CR cells exist in non-mammals but are extremely rare and thus were not sampled.

The non-mammalian CR cells show their highest density in the developing brain, suggesting they may play some role in pallial development like their mammalian counterparts. What exactly this ancestral CR function might be remains a matter of speculation, and will need to be addressed by functional studies. Here we find that *Reln* expression is not a conserved feature of vertebrate CR cells. This suggests that, if CR cells have a conserved function in all vertebrates, this function is Reln-independent. The gain of *Reln* expression late in CR cells evolution may have contributed to the emergence of mammalian-specific cortical features, such as radial migration and inside-out corticogenesis [1,6]. Indeed, *Reln* deletion in mouse *Tp73*+ CR cells affects cortical lamination, but does not recapitulate the other defects caused by CR cells genetic ablation [20,64]. Therefore, the regulation of radial migration by CR-derived Reln may have evolved with the transition from outside-in to inside-out corticogenesis, an innovation that took place in mammalian ancestors [40].

Besides regulating radial migration, mammalian CR cells have prominent roles in the assembly and maturation of neural circuits in the hippocampus [15,21–23] and neocortex [24]. In neocortical layer 1, CR cells are part of large networks of spontaneously-active neurons [25], and regulate the spatial distribution of superficial layer interneurons and dendritic maturation in pyramidal neurons [8]. In mammals, amphibians, non-avian reptiles, and certain fish species, the superficial neuropil layer (layer 1 in mammals) is a conserved site of integration of long-range inputs from cortical and subcortical areas, including sensory inputs relayed by thalamus [46,65]. Thus, the modulation of circuit assembly might have been an ancestral function of CR cells [17,66].

Intriguingly, thalamic spontaneous activity regulates CR density in mouse layer 1 [17]. It is tempting to speculate that the density of CR cells coevolved with the presence of sensory thalamic projections to the pallium, which are scarce in amphibians and seem more prominent in cartilagineous fishes [67,68], where CR cells are particularly abundant during development.

Finally, our results reveal a surprising degree of transcriptomic similarity between CR cells and OB *Tp73*+ ETCs. Several observations suggest that CR cells and ETCs are sister cell types, evolved from an ancestral cell type present in the last common ancestor of vertebrates (or earlier) (Fig. 6D). First, in mouse and salamander these two cell types share the expression of a long list of TFs previously thought to be CR-specific, indicating that their transcriptomic similarity is based on a largely shared regulatory program, therefore is not likely to be a result of convergent evolution. Second, lineage tracing experiments in mice indicate that some ETCs are born from pallial progenitors and then migrate to the OB, suggesting that CR and ETC cells may have a shared developmental origin [50,51]. Third, CR and ETCs have similar electrophysiological properties: they receive strong inputs from GABAergic interneurons, display synchronous bursting, have prominent inward rectifying currents, and are connected by gap junctions [4,52,53,69–71]. Fourth, both cell types have strong connections with the olfactory system: ETCs are directly postsynaptic to olfactory sensory neurons, whereas CR cells in the lateral olfactory tract, which function as guidepost neurons during development, seemingly belong to a population of lateral olfactory tract cells that receive second-order olfactory inputs from the bulb [72]. We thus propose that CR and ETCs may have evolved by duplication and divergence from cells involved in early olfactory processing in vertebrate ancestors. Our TF analysis suggests that CR cells may have evolved by neofunctionalization, by acquiring the expression of *Zic* and NFI transcription factors. This regulatory change may have conferred these cell new signaling functions to regulate circuit assembly in an expanded telencephalon [73], further supporting the hypothesis that olfactory circuits in ancestral vertebrates served as a developmental and functional blueprint for the evolving telencephalon (Fig. 6D).

Taken together, our findings also highlight the complex relationships between molecular and phenotypic cell type evolution[55]. Across vast evolutionary time, molecular signatures that define cell identity, such as transcription factor expression, may be preserved even when functional roles have diverged dramatically. Our study demonstrates how in-depth analyses of anatomical, transcriptomic, and developmental data can be used to identify and explain these unexpected evolutionary relationships.

Acknowledgements

We thank Nandan Nerurkar and Elanur Yilmaz (Columbia University) for providing chick and zebrafish samples, the Columbia ICM team for excellent animal care. We also thank Tosches lab members as well as Oliver Hobert and Hynek Wichterle for feedback throughout the project. Light-sheet imaging was performed with support from the Zuckerman Institute's Cellular Imaging platform (NIH grant 1S10OD023587-01). Computing resources were provided by Columbia University's

Shared Research Computing Facility (NIH grant 1G20RR030893-01 and NYSTAR contract C090171).

Funding: This work was supported by the National Institute of Health (grants NIGMS R35GM146973 and NHGRI RM1HG011014), the Rita Allen Foundation, and the Chan Zuckerberg Initiative (M.A.T.), the National Science Foundation (Graduate Research Fellowship to E.G.), the Revson Foundation (G.G.), an EMBO Long-Term Fellowship (A.D.), the Karen Toffler Charitable Trust Scholar Program (P.B.), and the Thompson Family Foundation Program for Accelerated Medicine Exploration in Alzheimer's Disease and Related Disorders of the Nervous System (TAME-AD) (C.K.).

Author Contributions: M.A.T. supervised the study. E.G., G.G., A.D, M.A.T. analyzed scRNA-seq data, and E.G. performed cross-species comparisons. E.G., G.G., P. B., J A.G., C.K. and J.W. prepared samples for histology. E.G., G.G., and J.W., performed histology and imaging. E.G. and M.A.T. wrote the manuscript, with edits from G.G., J.W., A.D., and C.K.

References

1. García-Moreno, F., and Molnár, Z. (2020). Variations of telencephalic development that paved the way for neocortical evolution. Prog. Neurobiol. *194*, 101865.

2. Goffinet, A.M. (2017). The evolution of cortical development: the synapsid-diapsid divergence. Development *144*, 4061–4077.

3. Elorriaga, V., Pierani, A., and Causeret, F. (2023). Cajal-retzius cells: Recent advances in identity and function. Curr. Opin. Neurobiol. *79*, 102686.

4. Kirischuk, S., Luhmann, H.J., and Kilb, W. (2014). Cajal-Retzius cells: update on structural and functional properties of these mystic neurons that bridged the 20th century. Neuroscience *275*, 33–46.

5. Causeret, F., Moreau, M.X., Pierani, A., and Blanquie, O. (2021). The multiple facets of Cajal-Retzius neurons. Development *148*, dev199409.

6. Marín-Padilla, M. (1998). Cajal–Retzius cells and the development of the neocortex. Copyright © *21*.

7. García-Moreno, F., López-Mascaraque, L., and De Carlos, J.A. (2007). Origins and migratory routes of murine Cajal-Retzius cells. J. Comp. Neurol. *500*, 419–432.

8. de Frutos, C.A., Bouvier, G., Arai, Y., Thion, M.S., Lokmane, L., Keita, M., Garcia-Dominguez, M., Charnay, P., Hirata, T., Riethmacher, D., et al. (2016). Reallocation of Olfactory Cajal-Retzius Cells Shapes Neocortex Architecture. Neuron *92*, 435–448.

487 9. Ruiz-Reig, N., Andrés, B., Huilgol, D., Grove, E.A., Tissir, F., Tole, S., Theil, T.,
488 Herrera, E., and Fairén, A. (2017). Lateral Thalamic Eminence: A Novel Origin for
489 mGluR1/Lot Cells. Cereb. Cortex *27*, 2841–2856.

490 10. Bielle, F., Griveau, A., Narboux-Nême, N., Vigneau, S., Sigrist, M., Arber, S.,
491 Wassef, M., and Pierani, A. (2005). Multiple origins of Cajal-Retzius cells at the borders
492 of the developing pallium. Nat. Neurosci. *8*, 1002–1012.

493 11. Takiguchi-Hayashi, K., Sekiguchi, M., Ashigaki, S., Takamatsu, M., Hasegawa,
494 H., Suzuki-Migishima, R., Yokoyama, M., Nakanishi, S., and Tanabe, Y. (2004).
495 Generation of reelin-positive marginal zone cells from the caudomedial wall of
496 telencephalic vesicles. J. Neurosci. *24*, 2286–2295.

497 12. Meyer, G., Perez-Garcia, C.G., Abraham, H., and Caput, D. (2002). Expression
498 of p73 and Reelin in the developing human cortex. J. Neurosci. *22*, 4973–4986.

499 13. D'Arcangelo, G., Miao, G.G., Chen, S.C., Soares, H.D., Morgan, J.I., and Curran,
500 T. (1995). A protein related to extracellular matrix proteins deleted in the mouse mutant
501 reeler. Nature *374*, 719–723.

502 14. Ogawa, M., Miyata, T., Nakajima, K., Yagyu, K., Seike, M., Ikenaka, K.,
503 Yamamoto, H., and Mikoshiba, K. (1995). The reeler gene-associated antigen on Cajal-
504 Retzius neurons is a crucial molecule for laminar organization of cortical neurons.
505 Neuron *14*, 899–912.

506 15. Del Río, J.A., Heimrich, B., Borrell, V., Förster, E., Drakew, A., Alcántara, S.,
507 Nakajima, K., Miyata, T., Ogawa, M., Mikoshiba, K., et al. (1997). A role for Cajal-
508 Retzius cells and reelin in the development of hippocampal connections. Nature *385*,
509 70–74.

510 16. Supèr, H., Martínez, A., Del Río, J.A., and Soriano, E. (1998). Involvement of
511 distinct pioneer neurons in the formation of layer-specific connections in the
512 hippocampus. J. Neurosci. *18*, 4616–4626.

513 17. Genescu, I., Aníbal-Martínez, M., Kouskoff, V., Chenouard, N., Mailhes-Hamon,
514 C., Cartonnet, H., Lokmane, L., Rijli, F.M., López-Bendito, G., Gambino, F., et al.
515 (2022). Dynamic interplay between thalamic activity and Cajal-Retzius cells regulates
516 the wiring of cortical layer 1. Cell Rep. *39*, 110667.

517 18. Barber, M., Arai, Y., Morishita, Y., Vigier, L., Causeret, F., Borello, U., Ledonne,
518 F., Coppola, E., Contremoulins, V., Pfrieger, F.W., et al. (2015). Migration speed of
519 Cajal-Retzius cells modulated by vesicular trafficking controls the size of higher-order
520 cortical areas. Curr. Biol. *25*, 2466–2478.

521 19. Alcántara, S., Pozas, E., Ibañez, C.F., and Soriano, E. (2006). BDNF-modulated
522 spatial organization of Cajal-Retzius and GABAergic neurons in the marginal zone plays
523 a role in the development of cortical organization. Cereb. Cortex *16*, 487–499.

20. Elorriaga, V., Bouloudi, B., Saillour, Y., Morel, J.S., Delberghe, E., Azzam, P., Moreau, M.X., Stottmann, R., Bahi-Buisson, N., Pierani, A., et al. (2024). Differential contribution of P73+ Cajal-Retzius cells and Reelin to cortical morphogenesis. bioRxiv. https://doi.org/10.1101/2024.10.15.618167.

21. Glærum, I.L., Dunville, K., Moan, K., Krause, M., Montaldo, N.P., Kirikae, H., Nigro, M.J., Sætrom, P., van Loon, B., and Quattrocolo, G. (2024). Postnatal persistence of hippocampal Cajal-Retzius cells has a crucial role in the establishment of the hippocampal circuit. Development *151*, dev202236.

22. Anstötz, M., Lee, S.K., and Maccaferri, G. (2022). Glutamate released by Cajal-Retzius cells impacts specific hippocampal circuits and behaviors. Cell Rep. *39*, 110822.

23. Riva, M., Moriceau, S., Morabito, A., Dossi, E., Sanchez-Bellot, C., Azzam, P., Navas-Olive, A., Gal, B., Dori, F., Cid, E., et al. (2023). Aberrant survival of hippocampal Cajal-Retzius cells leads to memory deficits, gamma rhythmopathies and susceptibility to seizures in adult mice. Nat. Commun. *14*, 1531.

24. Choe, Y., Siegenthaler, J.A., and Pleasure, S.J. (2012). A cascade of morphogenic signaling initiated by the meninges controls corpus callosum formation. Neuron *73*, 698–712.

25. Aguiló, A., Schwartz, T.H., Kumar, V.S., Peterlin, Z.A., Tsiola, A., Soriano, E., and Yuste, R. (1999). Involvement of cajal-retzius neurons in spontaneous correlated activity of embryonic and postnatal layer 1 from wild-type and reeler mice. J. Neurosci. *19*, 10856–10868.

26. Meyer, G., Socorro, A.C., Garcia, C.G.P., Millan, L.M., Walker, N., and Caput, D. (2004). Developmental Roles of p73 in Cajal-Retzius Cells and Cortical Patterning. J. Neurosci. *24*, 9878–9887.

27. Cabrera-Socorro, A., Hernandez-Acosta, N.C., Gonzalez-Gomez, M., and Meyer, G. (2007). Comparative aspects of p73 and Reelin expression in Cajal-Retzius cells and the cortical hem in lizard, mouse and human. Brain Res. *1132*, 59–70.

28. Tissir, F., Lambert De Rouvroit, C., Sire, J.-Y., Meyer, G., and Goffinet, A.M. (2003). Reelin expression during embryonic brain development in Crocodylus niloticus. J. Comp. Neurol. *457*, 250–262.

29. Moreau, M.X., Saillour, Y., Elorriaga, V., Bouloudi, B., Delberghe, E., Deutsch Guerrero, T., Ochandorena-Saa, A., Maeso-Alonso, L., Marques, M.M., Marin, M.C., et al. (2023). Repurposing of the multiciliation gene regulatory network in fate specification of Cajal-Retzius neurons. Dev. Cell *58*, 1365–1382.e6.

30. Jiménez, S., and Moreno, N. (2022). Analysis of the expression pattern of Cajal-Retzius cell markers in the Xenopus laevis forebrain. Brain Behav. Evol. *96*, 263–282.

31. Nomura, T., Takahashi, M., Hara, Y., and Osumi, N. (2008). Patterns of neurogenesis and amplitude of Reelin expression are essential for making a mammalian-type cortex. PLoS One *3*, e1454.

32. García-Moreno, F., Anderton, E., Jankowska, M., Begbie, J., Encinas, J.M., Irimia, M., and Molnár, Z. (2018). Absence of tangentially migrating glutamatergic neurons in the developing avian brain. Cell Rep. *22*, 96–109.

33. Moreau, M.X., Saillour, Y., Cwetsch, A.W., Pierani, A., and Causeret, F. (2021). Single-cell transcriptomics of the early developing mouse cerebral cortex disentangle the spatial and temporal components of neuronal fate acquisition. Development *148*. https://doi.org/10.1242/dev.197962.

34. Rentzsch, F., Kramer, C., and Hammerschmidt, M. (2003). Specific and conserved roles of TAp73 during zebrafish development. Gene *323*, 19–30.

35. Tissir, F., Ravni, A., Achouri, Y., Riethmacher, D., Meyer, G., and Goffinet, A.M. (2009). DeltaNp73 regulates neuronal survival in vivo. Proceedings of the National Academy of Sciences *106*, 16871–16876.

36. Yang, A., Walker, N., Bronson, R., Kaghad, M., Oosterwegel, M., Bonnin, J., Vagner, C., Bonnet, H., Dikkes, P., Sharpe, A., et al. (2000). P73-deficient mice have neurological, pheromonal and inflammatory defects but lack spontaneous tumours. Nature *404*, 99–103.

37. Schiffmann, S.N., Bernier, B., and Goffinet, A.M. (1997). Reelin mRNA expression during mouse brain development. Eur. J. Neurosci. *9*, 1055–1071.

38. Joven, A., Wang, H., Pinheiro, T., Hameed, L.S., Belnoue, L., and Simon, A. (2018). Cellular basis of brain maturation and acquisition of complex behaviors in salamanders. Development *145*, dev160051.

39. Yao, Z., van Velthoven, C.T.J., Kunst, M., Zhang, M., McMillen, D., Lee, C., Jung, W., Goldy, J., Abdelhak, A., Aitken, M., et al. (2023). A high-resolution transcriptomic and spatial atlas of cell types in the whole mouse brain. Nature *624*, 317–332.

40. Deryckere A, Choudhary S, Lynch C, Limperis LK, Affatato P, Woych J, Gumnit E, Ortega Gurrola A, Satija R, Mayer C, Tosches MA (2025). A conserved logic for the development of cortical layering in tetrapods. bioRxiv. https://doi.org/10.1101/2025.10.01.679862.

41. La Manno, G., Siletti, K., Furlan, A., Gyllborg, D., Vinsland, E., Mossi Albiach, A., Mattsson Langseth, C., Khven, I., Lederer, A.R., Dratva, L.M., et al. (2021). Molecular architecture of the developing mouse brain. Nature *596*, 92–96.

596 42. Tosches, M.A., Yamawaki, T.M., Naumann, R.K., Jacobi, A.A., Tushev, G., and
597 Laurent, G. (2018). Evolution of pallium, hippocampus, and cortical cell types revealed
598 by single-cell transcriptomics in reptiles. Science *360*, 881–888.

599 43. Hao, Y., Hao, S., Andersen-Nissen, E., Mauck, W.M., 3rd, Zheng, S., Butler, A.,
600 Lee, M.J., Wilk, A.J., Darby, C., Zager, M., et al. (2021). Integrated analysis of
601 multimodal single-cell data. Cell *184*, 3573–3587.e29.

602 44. Pandey, S., Moyer, A.J., and Thyme, S.B. (2023). A single-cell transcriptome
603 atlas of the maturing zebrafish telencephalon. Genome Res. *33*, 658–671.

604 45. Anneser, L., Satou, C., Hotz, H.-R., and Friedrich, R.W. (2024). Molecular
605 organization of neuronal cell types and neuromodulatory systems in the zebrafish
606 telencephalon. Curr. Biol. *34*, 298–312.e4.

607 46. Woych, J., Ortega Gurrola, A., Deryckere, A., Jaeger, E.C.B., Gumnit, E.,
608 Merello, G., Gu, J., Joven Araus, A., Leigh, N.D., Yun, M., et al. (2022). Cell-type
609 profiling in salamanders identifies innovations in vertebrate forebrain evolution. Science
610 *377*, eabp9186.

611 47. Zeppilli, S., Ackels, T., Attey, R., Klimpert, N., Ritola, K.D., Boeing, S.,
612 Crombach, A., Schaefer, A.T., and Fleischmann, A. (2021). Molecular characterization
613 of projection neuron subtypes in the mouse olfactory bulb. Elife *10*, e65445.

614 48. Lein, E.S., Hawrylycz, M.J., Ao, N., Ayres, M., Bensinger, A., Bernard, A., Boe,
615 A.F., Boguski, M.S., Brockway, K.S., Byrnes, E.J., et al. (2007). Genome-wide atlas of
616 gene expression in the adult mouse brain. Nature *445*, 168–176.

617 49. Tufo, C., Poopalasundaram, S., Dorrego-Rivas, A., Ford, M.C., Graham, A., and
618 Grubb, M.S. (2022). Development of the mammalian main olfactory bulb. Development
619 *149*, dev200210.

620 50. Winpenny, E., Lebel-Potter, M., Fernandez, M.E., Brill, M.S., Götz, M., Guillemot,
621 F., and Raineteau, O. (2011). Sequential generation of olfactory bulb glutamatergic
622 neurons by Neurog2-expressing precursor cells. Neural Dev. *6*, 12.

623 51. Roybon, L., Mastracci, T.L., Li, J., Stott, S.R.W., Leiter, A.B., Sussel, L., Brundin,
624 P., and Li, J.-Y. (2015). The Origin, Development and Molecular Diversity of Rodent
625 Olfactory Bulb Glutamatergic Neurons Distinguished by Expression of Transcription
626 Factor NeuroD1. PLoS One *10*, e0128035.

627 52. Antal, M., Eyre, M., Finklea, B., and Nusser, Z. (2006). External tufted cells in the
628 main olfactory bulb form two distinct subpopulations. Eur. J. Neurosci. *24*, 1124–1136.

629 53. Tatti, R., Bhaukaurally, K., Gschwend, O., Seal, R.P., Edwards, R.H., Rodriguez,
630 I., and Carleton, A. (2014). A population of glomerular glutamatergic neurons controls
631 sensory information transfer in the mouse olfactory bulb. Nat. Commun. *5*, 3791.

632 54. Zaremba, B., Fallahshahroudi, A., Schneider, C., Schmidt, J., Sarropoulos, I.,
633 Leushkin, E., Berki, B., Van Poucke, E., Jensen, P., Senovilla-Ganzo, R., et al. (2025).
634 Developmental origins and evolution of pallial cell types and structures in birds. Science
635 *387*, eadp5182.

636 55. Arendt, D., Musser, J.M., Baker, C.V.H., Bergman, A., Cepko, C., Erwin, D.H.,
637 Pavlicev, M., Schlosser, G., Widder, S., Laubichler, M.D., et al. (2016). The origin and
638 evolution of cell types. Nat. Rev. Genet. *17*, 744–757.

639 56. Murillo, B., Ruiz-Reig, N., Herrera, M., Fairén, A., and Herrera, E. (2015). Zic2
640 Controls the Migration of Specific Neuronal Populations in the Developing Forebrain. J.
641 Neurosci. *35*, 11266–11280.

642 57. Borrell, V., and Marín, O. (2006). Meninges control tangential migration of hem-
643 derived Cajal-Retzius cells via CXCL12/CXCR4 signaling. Nat. Neurosci. *9*, 1284–1293.

644 58. Gil-Sanz, C., Franco, S.J., Martinez-Garay, I., Espinosa, A., Harkins-Perry, S.,
645 and Müller, U. (2013). Cajal-Retzius cells instruct neuronal migration by coincidence
646 signaling between secreted and contact-dependent guidance cues. Neuron *79*, 461–
647 477.

648 59. Yamazaki, H., Sekiguchi, M., Takamatsu, M., Tanabe, Y., and Nakanishi, S.
649 (2004). Distinct ontogenic and regional expressions of newly identified Cajal-Retzius
650 cell-specific genes during neocorticogenesis. Proceedings of the National Academy of
651 Sciences *101*, 14509–14514.

652 60. Saulnier, A., Keruzore, M., De Clercq, S., Bar, I., Moers, V., Magnani, D.,
653 Walcher, T., Filippis, C., Kricha, S., Parlier, D., et al. (2013). The doublesex homolog
654 Dmrt5 is required for the development of the caudomedial cerebral cortex in mammals.
655 Cereb. Cortex *23*, 2552–2567.

656 61. Huilgol, D., Udin, S., Shimogori, T., Saha, B., Roy, A., Aizawa, S., Hevner, R.F.,
657 Meyer, G., Ohshima, T., Pleasure, S.J., et al. (2013). Dual origins of the mammalian
658 accessory olfactory bulb revealed by an evolutionarily conserved migratory stream. Nat.
659 Neurosci. *16*, 157–165.

660 62. Alonso, A., Trujillo, C.M., and Puelles, L. (2020). Longitudinal developmental
661 analysis of prethalamic eminence derivatives in the chick by mapping of Tbr1 in situ
662 expression. Brain Struct. Funct. *225*, 481–510.

663 63. Quintana-Urzainqui, I., Oel, P.A., Gerber, T., Pan, L., Papadopoulos, N., Serka,
664 Z.G., Verbanac, A., Börsig, M., Torres-Sabino, D., Rollán-Delgado, I.C., et al. (2025).
665 Developmental landscape of shark telencephalon sheds light on the evolution of
666 telencephalic cell types and the ancient origin of Cajal-Retzius cells. bioRxiv,
667 2025.05.08.652169. https://doi.org/10.1101/2025.05.08.652169.

668 64. Vílchez-Acosta, A., Manso, Y., Cárdenas, A., Elias-Tersa, A., Martínez-Losa, M.,
669 Pascual, M., Álvarez-Dolado, M., Nairn, A.C., Borrell, V., and Soriano, E. (2022).

670 Specific contribution of Reelin expressed by Cajal–Retzius cells or GABAergic
671 interneurons to cortical lamination. Proceedings of the National Academy of Sciences
672 *119*, e2120079119.

673 65. Fournier, J., Müller, C.M., and Laurent, G. (2015). Looking for the roots of cortical
674 sensory computation in three-layered cortices. Curr. Opin. Neurobiol. *31*, 119–126.

675 66. Damilou, A., Cai, L., Argunşah, A.Ö., Han, S., Kanatouris, G., Karatsoli, M.,
676 Hanley, O., Gesuita, L., Kollmorgen, S., Helmchen, F., et al. (2024). Developmental
677 Cajal-Retzius cell death contributes to the maturation of layer 1 cortical inhibition and
678 somatosensory processing. Nat. Commun. *15*, 6501.

679 67. Striedter, G.F., and Northcutt, R.G. (2022). The independent evolution of dorsal
680 pallia in multiple vertebrate lineages. Brain Behav. Evol. *96*, 200–211.

681 68. Bodznick, D., and Northcutt, R.G. (1984). An electrosensory area in the
682 telencephalon of the little skate, Raja erinacea. Brain Res. *298*, 117–124.

683 69. Hayar, A., Shipley, M.T., and Ennis, M. (2005). Olfactory bulb external tufted
684 cells are synchronized by multiple intraglomerular mechanisms. J. Neurosci. *25*, 8197–
685 8208.

686 70. Quattrocolo, G., and Maccaferri, G. (2013). Novel GABAergic circuits mediating
687 excitation/inhibition of Cajal-Retzius cells in the developing hippocampus. J. Neurosci.
688 *33*, 5486–5498.

689 71. Hayar, A., Karnup, S., Ennis, M., and Shipley, M.T. (2004). External tufted cells:
690 a major excitatory element that coordinates glomerular activity. J. Neurosci. *24*, 6676–
691 6685.

692 72. Hirata, T., Kumada, T., Kawasaki, T., Furukawa, T., Aiba, A., Conquet, F., Saga,
693 Y., and Fukuda, A. (2012). Guidepost neurons for the lateral olfactory tract: expression
694 of metabotropic glutamate receptor 1 and innervation by glutamatergic olfactory bulb
695 axons. Dev. Neurobiol. *72*, 1559–1576.

696 73. Molnár, Z., Luhmann, H.J., and Kanold, P.O. (2020). Transient cortical circuits
697 match spontaneous and sensory-driven activity during development. Science *370*,
698 eabb2153.

699 74. Arendt, D. (2008). The evolution of cell types in animals: emerging principles
700 from molecular studies. Nat. Rev. Genet. *9*, 868–882.

701 75. Puopolo, M., and Belluzzi, O. (1998). Inhibitory synapses among interneurons in
702 the glomerular layer of rat and frog olfactory bulbs. J. Neurophysiol. *80*, 344–349.

703 76. Marín-Padilla, M. (1990). Three-dimensional structural organization of layer I of
704 the human cerebral cortex: a Golgi study. J. Comp. Neurol. *299*, 89–105.

77. Gallien L, D.M. (1957). Table chronologique du développement chez Pleurodeles Waltlii Michah. Bull. Bio.

78. Hamburger, V., and Hamilton, H.L. (1992). A series of normal stages in the development of the chick embryo. 1951. Dev. Dyn. *195*, 231–272.

79. Gillis, J.A., Bennett, S., Criswell, K.E., Rees, J., Sleight, V.A., Hirschberger, C., Calzarette, D., Kerr, S., and Dasen, J. (2022). Big insight from the little skate: Leucoraja erinacea as a developmental model system. Curr. Top. Dev. Biol. *147*, 595–630.

80. Andreatta, M., and Carmona, S.J. (2021). UCell: Robust and scalable single-cell gene signature scoring. Comput. Struct. Biotechnol. J. *19*, 3796–3798.

81. Svara, F., Förster, D., Kubo, F., Januszewski, M., Dal Maschio, M., Schubert, P.J., Kornfeld, J., Wanner, A.A., Laurell, E., Denk, W., et al. (2022). Automated synapse-level reconstruction of neural circuits in the larval zebrafish brain. Nat. Methods *19*, 1357–1366.

82. Cantalapiedra, C.P., Hernández-Plaza, A., Letunic, I., Bork, P., and Huerta-Cepas, J. (2021). EggNOG-mapper v2: Functional annotation, orthology assignments, and domain prediction at the metagenomic scale. Mol. Biol. Evol. *38*, 5825–5829.

83. Choi, H.M.T., Schwarzkopf, M., Fornace, M.E., Acharya, A., Artavanis, G., Stegmaier, J., Cunha, A., and Pierce, N.A. (2018). Third-generation in situ hybridization chain reaction: multiplexed, quantitative, sensitive, versatile, robust. Development *145*, dev165753.

84. Jaeger, E.C.B., Vijatovic, D., Deryckere, A., Zorin, N., Nguyen, A.L., Ivanian, G., Woych, J., Arnold, R.C., Gurrola, A.O., Shvartsman, A., et al. (2025). Adeno-associated viral tools to trace neural development and connectivity across amphibians. Dev. Cell *60*, 794–812.e6.

85. Kuehn, E., Clausen, D.S., Null, R.W., Metzger, B.M., Willis, A.D., and Özpolat, B.D. (2022). Segment number threshold determines juvenile onset of germline cluster expansion in Platynereis dumerilii. J. Exp. Zool. B Mol. Dev. Evol. *338*, 225–240.

86. Andrews, T.G.R., Gattoni, G., Busby, L., Schwimmer, M.A., and Benito-Gutiérrez, È. (2020). Hybridization chain reaction for quantitative and multiplex imaging of gene expression in amphioxus embryos and adult tissues. Methods Mol. Biol. *2148*, 179–194.

87. Wullimann, M.F., Mokayes, N., Shainer, I., Kuehn, E., and Baier, H. (2024). Genoarchitectonics of the larval zebrafish diencephalon. J. Comp. Neurol. *532*, e25549.

88. Kunst, M., Laurell, E., Mokayes, N., Kramer, A., Kubo, F., Fernandes, A.M., Förster, D., Dal Maschio, M., and Baier, H. (2019). A cellular-resolution atlas of the larval zebrafish brain. Neuron *103*, 21–38.e5.

740 89. Kenney, J.W., Steadman, P.E., Young, O., Shi, M.T., Polanco, M., Dubaishi, S.,
741 Covert, K., Mueller, T., and Frankland, P.W. (2021). A 3D adult zebrafish brain atlas
742 (AZBA) for the digital age. Elife *10*. https://doi.org/10.7554/eLife.69988.

743
744
745
746
747
748
749
750
751
752
753
754
755
756
757
758
759

Main Figures

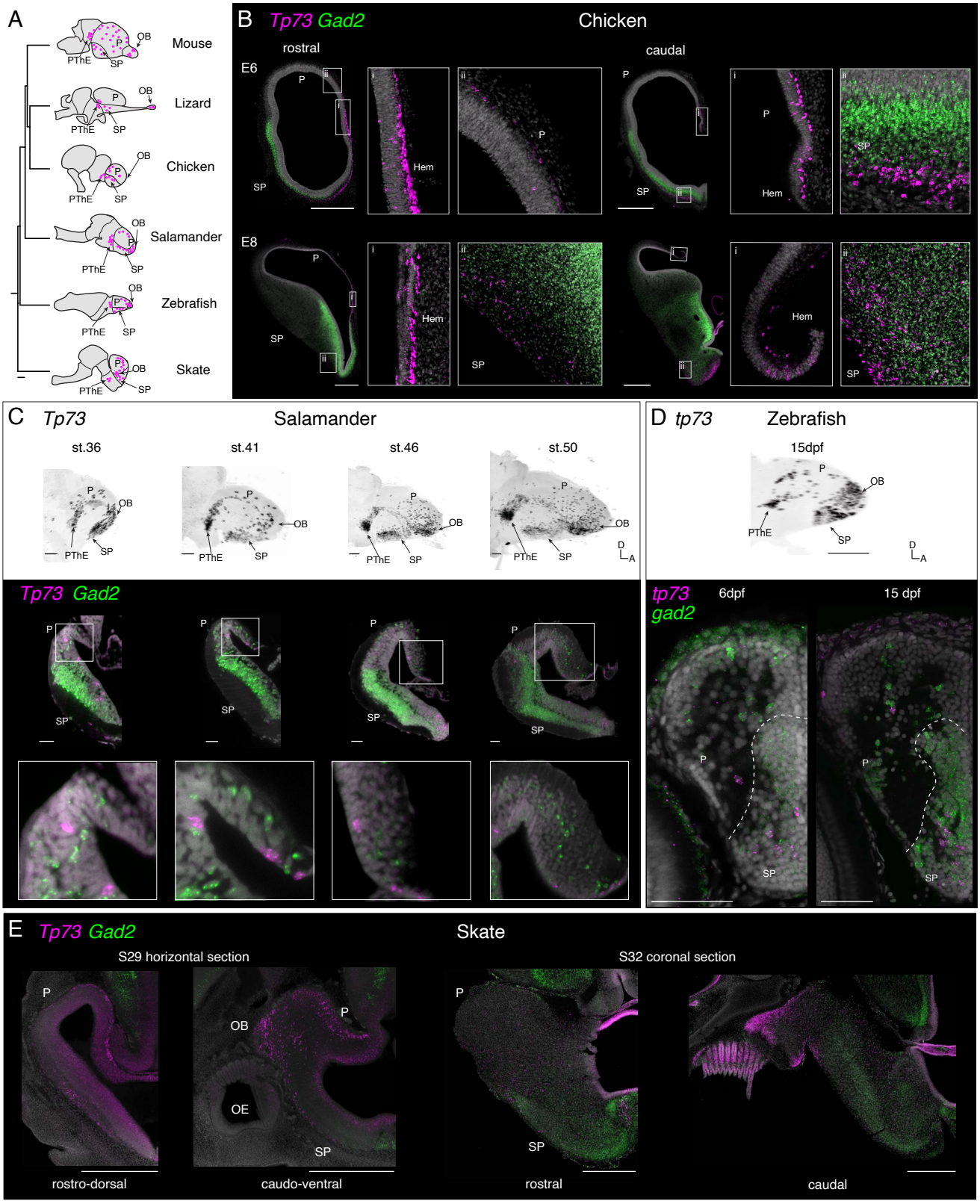

762 **Figure 1. Conserved *Tp73* expression in vertebrate forebrains.**
763 (A) Distribution of *Tp73* neurons in vertebrate brains, according to published data and
764 this study. Scale bar: 100 million years. (B) Double HCRs for *Tp73* (magenta) and *Gad2*
765 (green) in coronal sections of chick brains (embryonic stages E6 and E8), showing *Tp73*
766 expression in the developing hem, pallium, and subpallium. *Gad2* labels GABAergic
767 neurons and helps identify the pallial-subpallial boundary. Scale bars = 500 um. (C)
768 Top: 3D max intensity projections (lateral views, anterior on the right) of salamander
769 brains (larval stages 36, 41, 46, and 50) after whole mount HCR for *Tp73.* Scale bar
770 100um. Bottom: optical coronal sections through one telencephalic hemisphere of *Tp73*
771 and *Gad2*-labeled brains at different developmental stages; insets show *Tp73*+ and
772 *Gad2*+ neurons in pallium. Scale bar 50 um. (D) 3D max intensity projection of a whole
773 mount 15 dpf zebrafish brain (lateral view, anterior on the right) after HCR for *tp73.*
774 Scale bar 100 um. Bottom: sections of *tp73* and *gad2*-labeled 6 dpf and 15dpf zebrafish
775 brains showing *tp73*+ and *gad2*+ neurons in pallium and subpallium. Scale bar 50 um.
776 (E) Expression of *Tp73* and *Gad2* in the developing skate brain. Left: horizontal sections
777 of stage 29 brains; right: coronal sections of stage 32 brains. Scale bar 500um. See
778 additional sections in fig. S1.
779
780 Abbreviations: E, embryonic day; P, pallium; SP, subpallium; OB, olfactory bulb; OE,
781 olfactory epithelium; PThE, prethalamic eminence; dpf, days post fertilization; A,
782 anterior; D, dorsal.

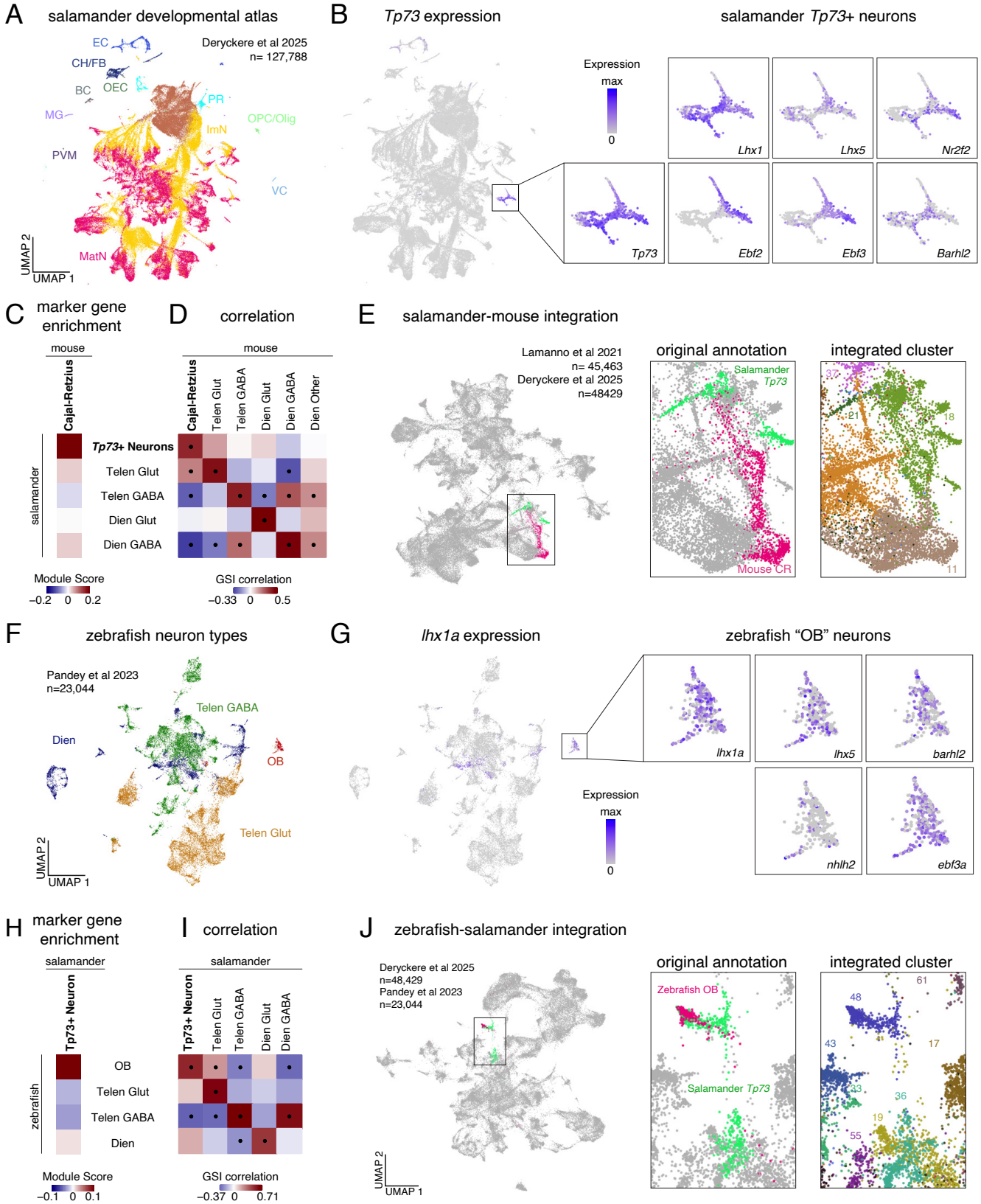
A
salamander developmental atlas
Deryckere et al 2025
n= 127,788
EC
CH/FB
BC
OEC
MG
PR
OPC/Olig
ImN
PVM
VC
MatN
UMAP 2
UMAP 1
B
Tp73 expression
salamander Tp73+ neurons
Expression
max
0
Lhx1
Lhx5
Nr2f2
Tp73
Ebf2
Ebf3
Barhl2
C
marker gene enrichment
mouse
Cajal-Retzius
salamander
Tp73+ Neurons
Telen Glut
Telen GABA
Dien Glut
Dien GABA
Module Score
−0.2 0 0.2
D
correlation
mouse
Cajal-Retzius
Telen Glut
Telen GABA
Dien Glut
Dien GABA
Dien Other
GSI correlation
−0.33 0 0.5
E
salamander-mouse integration
Lamanno et al 2021
n= 45,463
Deryckere et al 2025
n=48429
original annotation
Salamander
Tp73
Mouse CR
integrated cluster
37
21
18
13
11
F
zebrafish neuron types
Pandey et al 2023
n=23,044
Telen GABA
Dien
OB
Telen Glut
UMAP 2
UMAP 1
G
lhx1a expression
zebrafish "OB" neurons
lhx1a
lhx5
barhl2
nhlh2
ebf3a
Expression
max
0
H
marker gene enrichment
salamander
Tp73+ Neuron
zebrafish
OB
Telen Glut
Telen GABA
Dien
Module Score
−0.1 0 0.1
I
correlation
salamander
Tp73+ Neuron
Telen Glut
Telen GABA
Dien Glut
Dien GABA
GSI correlation
−0.37 0 0.71
J
zebrafish-salamander integration
Deryckere et al 2025
n=48,429
Pandey et al 2023
n=23,044
UMAP 2
UMAP 1
original annotation
Zebrafish OB
Salamander Tp73
integrated cluster
61
48
43
17
33
36
19
55

783
784

785 **Figure 2. Mouse, salamander, and zebrafish *Tp73*+ neurons have a shared**
786 **transcriptomic signature.**
787 (A) UMAP of the Deryckere et al. [40] scRNA-seq dataset from the developing
788 salamander brain (n=127,788 cells), showing cells colored by broad class. (B) Left:
789 UMAP showing *Tp73* expression in the developing salamander brain dataset. Right:
790 Zoom on *Tp73*+ neurons, showing the expression of known CR marker TFs [5] (fig. S3A
791 for full UMAPs of zoomed genes). (C) Expression enrichment of mouse CR cell markers
792 (Seurat Module Score) in salamander cell classes. Module score computed for the top
793 49 CR markers in La Manno et al [41] (see Methods for gene selection criteria). (D)
794 Pairwise GSI correlations of classes of salamander and mouse forebrain neurons
795 (mouse data from La Manno et al.[41]). Correlations based on the intersection of genes
796 that were differentially expressed in both mouse and salamander (336 total genes).
797 Dots indicate statistically significant correlations. (E) UMAP showing forebrain neurons
798 from developing salamander and mouse after Seurat CCA integration. Salamander
799 *Tp73*+ neurons and mouse CR cells highlighted in green and magenta, respectively.
800 Right: Zoom on integrated cluster 18 containing salamander *Tp73* neurons and mouse
801 CR cells. (F) UMAP of the Pandey et al 2023 [44] dataset from the developing zebrafish
802 telencephalon (n=23,044 cells, stages 6 and 15 dpf only), showing cells colored by
803 class. (G) Left: UMAP showing *lhx1a* expression in the larval zebrafish dataset. Right:
804 Zoom on zebrafish OB neurons showing expression of *lhx1a* and other CR TFs. (H)
805 Expression enrichment of salamander *Tp73*+ neurons markers (Seurat Module Score)
806 in zebrafish cell classes. Module score computed for the top 42 markers of salamander
807 *Tp73*+ neurons (see methods for gene selection criteria) (I) Pairwise GSI correlations of
808 salamander and zebrafish forebrain neuron classes. Correlations based on the
809 intersection of genes that were differentially expressed in both zebrafish and
810 salamander (143 total genes). Dots indicate statistically significant correlations. (J)
811 UMAP showing forebrain neurons from developing salamander and zebrafish after
812 Seurat CCA integration. Right: Zoom on integrated cluster 48 containing salamander
813 *Tp73* neurons and zebrafish OB cells.
814
815 Abbreviations: BC, blood cells; CH/FB, chondrocytes/fibroblasts; EC, epithelial cells;
816 Dien, diencephalon; GABA, GABAergic; Glut, glutamatergic; GSI, gene specificity index;
817 ImN, immature neurons; MatN, mature neurons; MG, microglia; OEC, olfactory
818 ensheathing cells; OPC/Olig, oligodendrocyte precursor cells/oligodendrocytes; PVM,
819 perivascular macrophages; PR, photoreceptor cells; RG, radial glia; Telen,
820 telencephalon; VC, vascular cells; see also Fig. 1.

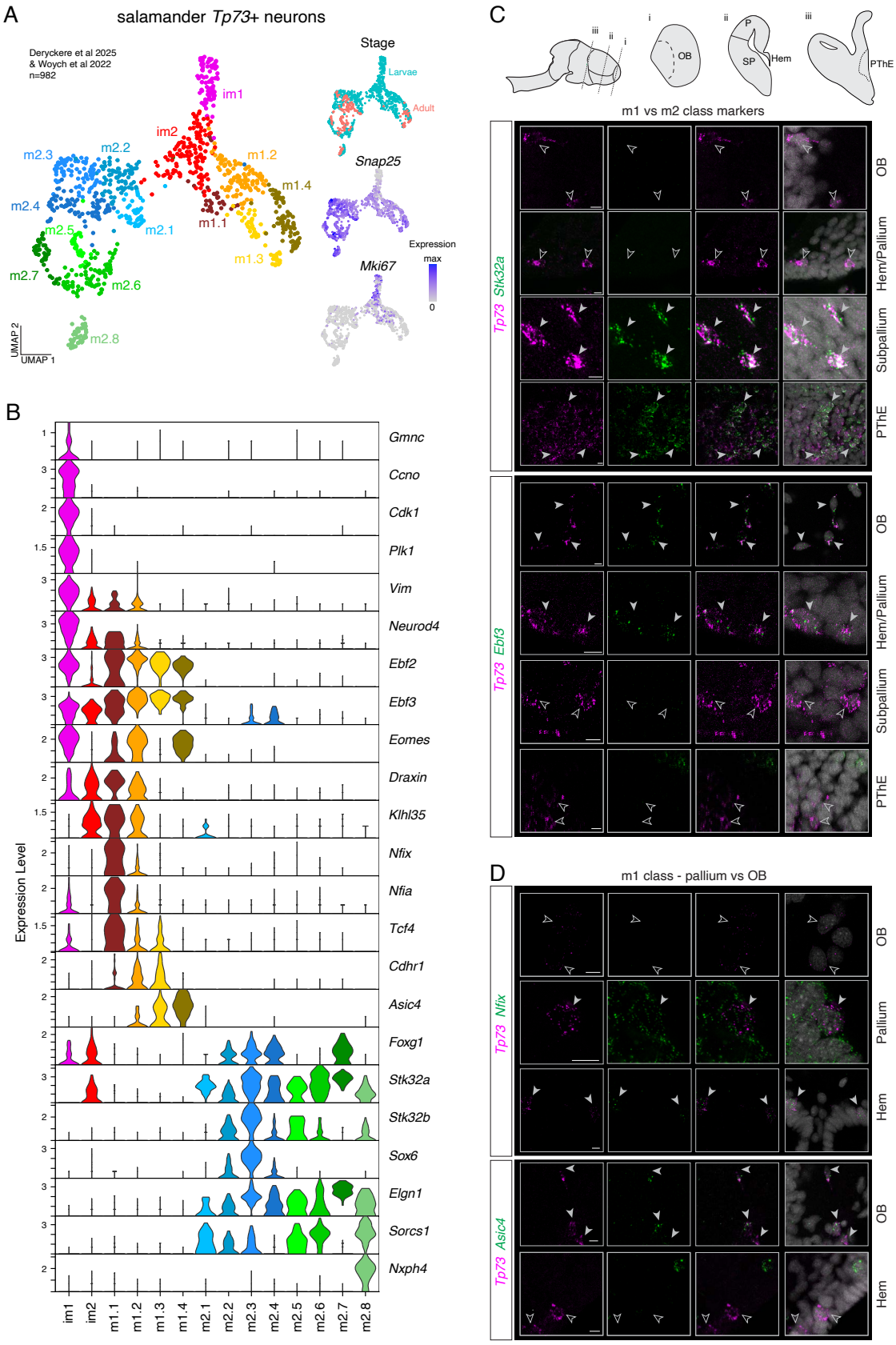
A
salamander Tp73+ neurons
Deryckere et al 2025
& Woych et al 2022
n=982
Stage
Larvae
Adult
Snap25
Mki67
Expression
max
0
im1
im2
m1.1
m1.2
m1.3
m1.4
m2.1
m2.2
m2.3
m2.4
m2.5
m2.6
m2.7
m2.8
UMAP 2
UMAP 1
B
Expression Level
Gmnc
Ccno
Cdk1
Plk1
Vim
Neurod4
Ebf2
Ebf3
Eomes
Draxin
Klhl35
Nfix
Nfia
Tcf4
Cdhr1
Asic4
Foxg1
Stk32a
Stk32b
Sox6
Elgn1
Sorcs1
Nxph4
C
OB
SP
P
Hem
PThE
m1 vs m2 class markers
Tp73 Stk32a
Tp73 Ebf3
OB
Hem/Pallium
Subpallium
PThE
D
m1 class - pallium vs OB
Tp73 Nfix
Tp73 Asic4
OB
Pallium
Hem

821

822 **Figure 3. Transcriptomic and spatial heterogeneity of salamander *Tp73+* neurons**
823 (A) UMAPs of the salamander *Tp73*+ neurons dataset (n= 982 cells). Left: *Tp73*+
824 neurons colored by cluster. Right: *Tp73*+ neurons colored by dataset (adult from Woych
825 et al [46]), and expression of *Snap25* and *Mki67*. (B) Violin plots showing the expression
826 of marker genes for *Tp73* neuronal clusters; m1 and m2 populations express different
827 sets of markers. (C)-(D) Closeups showing coexpression of *Tp73* and selected marker
828 genes detected by HCR in late active larvae (stages 46-55; see fig S8 for full images).
829 (C) Top: coexpression of *Stk32a* and *Tp73* in PthE and subpallium but not in OB and
830 hem/pallium. Bottom: *Ebf3* and *Tp73* coexpression in OB and hem/pallium but not
831 subpallium and PThEregions. Scale bar 10um. (D) Top: coexpression of *Nfix* and *Tp73*
832 in pallium but not OB. Bottom: coexpression of *Asic4* and *Tp73* in OB but not hem.
833 Scale bar: 10 um.
834
835 Abbreviations: im, immature; m, mature; see also Figure 1.
836

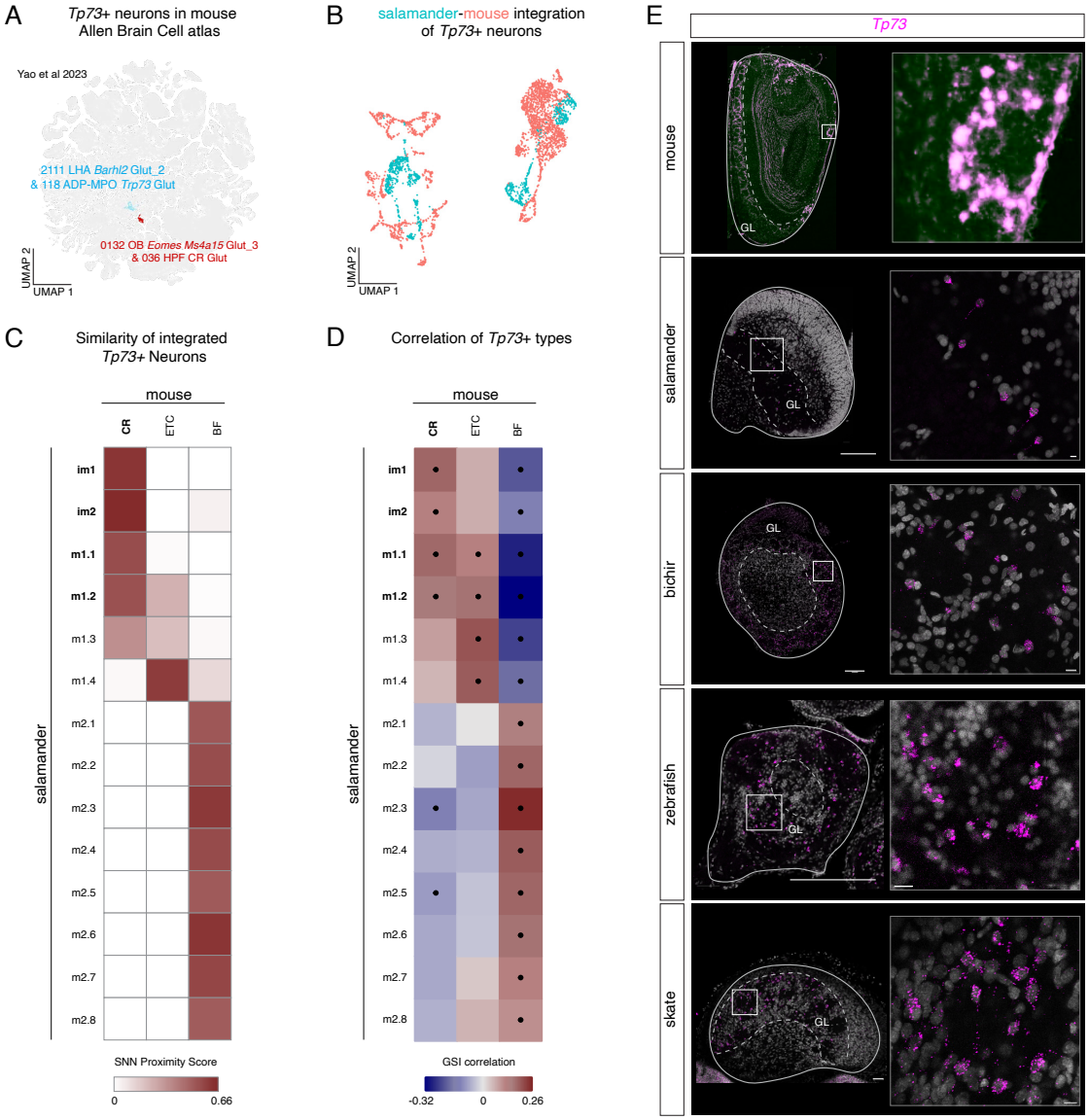

Figure 4. Transcriptomic similarity of CR and *Tp73*+ external tufted cells in mouse and salamander.

(A) UMAP of the mouse Allen Brain Cell atlas [39], highlighting the *Tp73*+ cells used for further analysis. (B) UMAPs showing salamander and mouse *Tp73*+ neurons after Seurat CCA integration, with cells colored by species. (C) Cross-species nearest neighbor proximity of mouse and salamander *Tp73*+ neurons in the integrated transcriptomic space. Higher score indicates higher reciprocal proximity of neurons of a given type in the integrated space (see Methods). (D) Pairwise GSI correlations of mouse and salamander *Tp73*+ types. Correlations based on the intersection of genes differentially expressed in both mouse and salamander (647 total). Dots indicate statistically significant correlations. (E).*Tp73*+ neurons in the OB glomerular layer of mouse (adult), salamander (adult), bichir fish (adult), zebrafish (3 mpf), and skate

852 (adult). Mouse *Trp73* colorimetric *in situ* hybridization adapted from mouse Allen Mouse
853 Brain Atlas, mouse.brain-map.org and atlas.brain-map.org [48]. All other images are *Tp73*
854 HCRs. Full image scale bars 200um. Zoom scale bars 10um.
855 Abbreviations: BF, basal forebrain; ETC, external tufted cells; GL, glomerular layer; see
856 also Figures 1, 2, and 3.
857
858
859
860
861
862
863
864
865
866
867
868
869
870
871
872
873
874
875
876
877

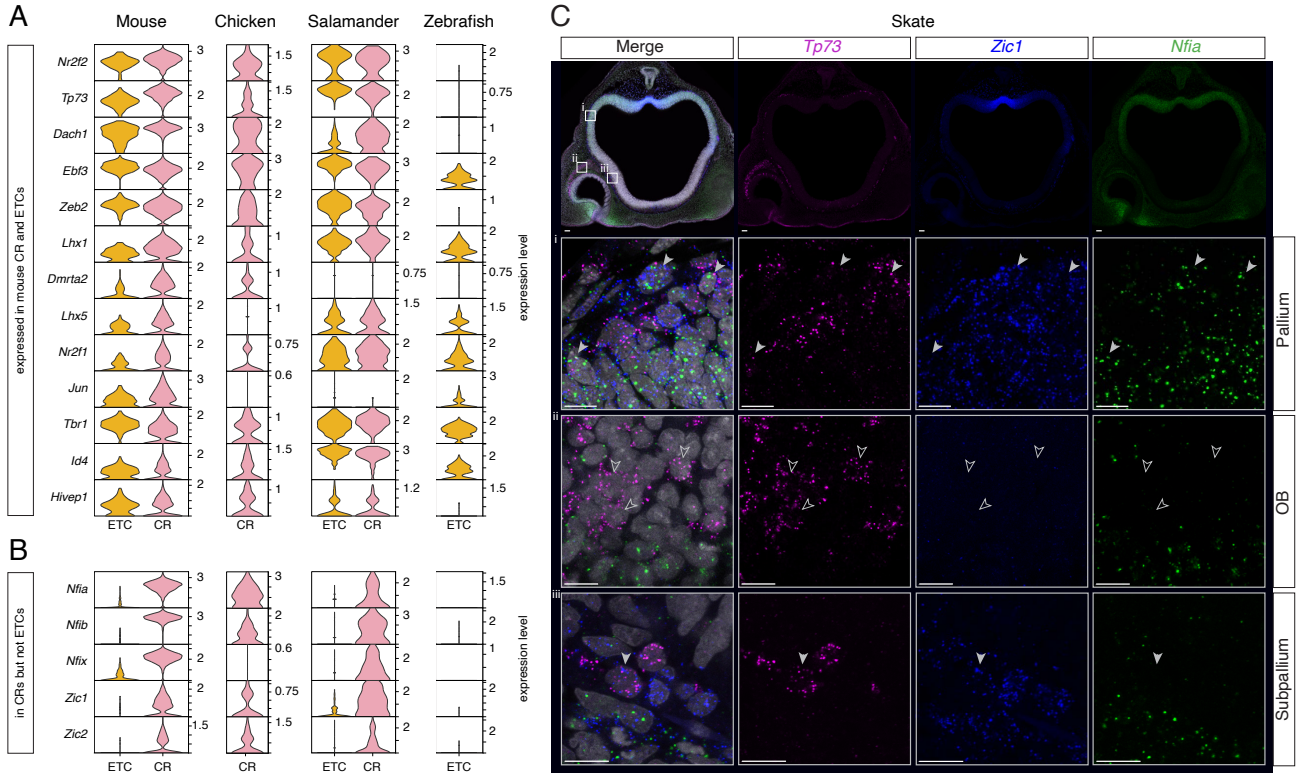

Figure 5. Transcription factor expression in CR cells and ETCs across vertebrates.
(A) Top: Violin plots showing expression of TFs expressed in both mouse CR cells and ETC compared to a cell type used as outgroup (OB mitral/tufted cells), and the expression of the same TFs in other vertebrate species. (B) Violin plots showing expression of TFs that differentiate CR cells and ETCs in both mouse and salamander, and the expression of the same TFs in chick CR cells and zebrafish ETCs. Data from [39,40,44,46,54] (see Methods for details). (C) HCR triple in situ hybridization for *Tp73*, *Zic1*, and *Nfia* in stage 29 skate telencephalon. (i) Coexpression of all three marker genes in pallial neurons suggesting a CR identity; (ii) *Tp73*+ in OB do not coexpress Zic1 and *Nfia*; (iii) coexpression of *Tp73* and *Zic1* but not *Nfia* in subpallium.

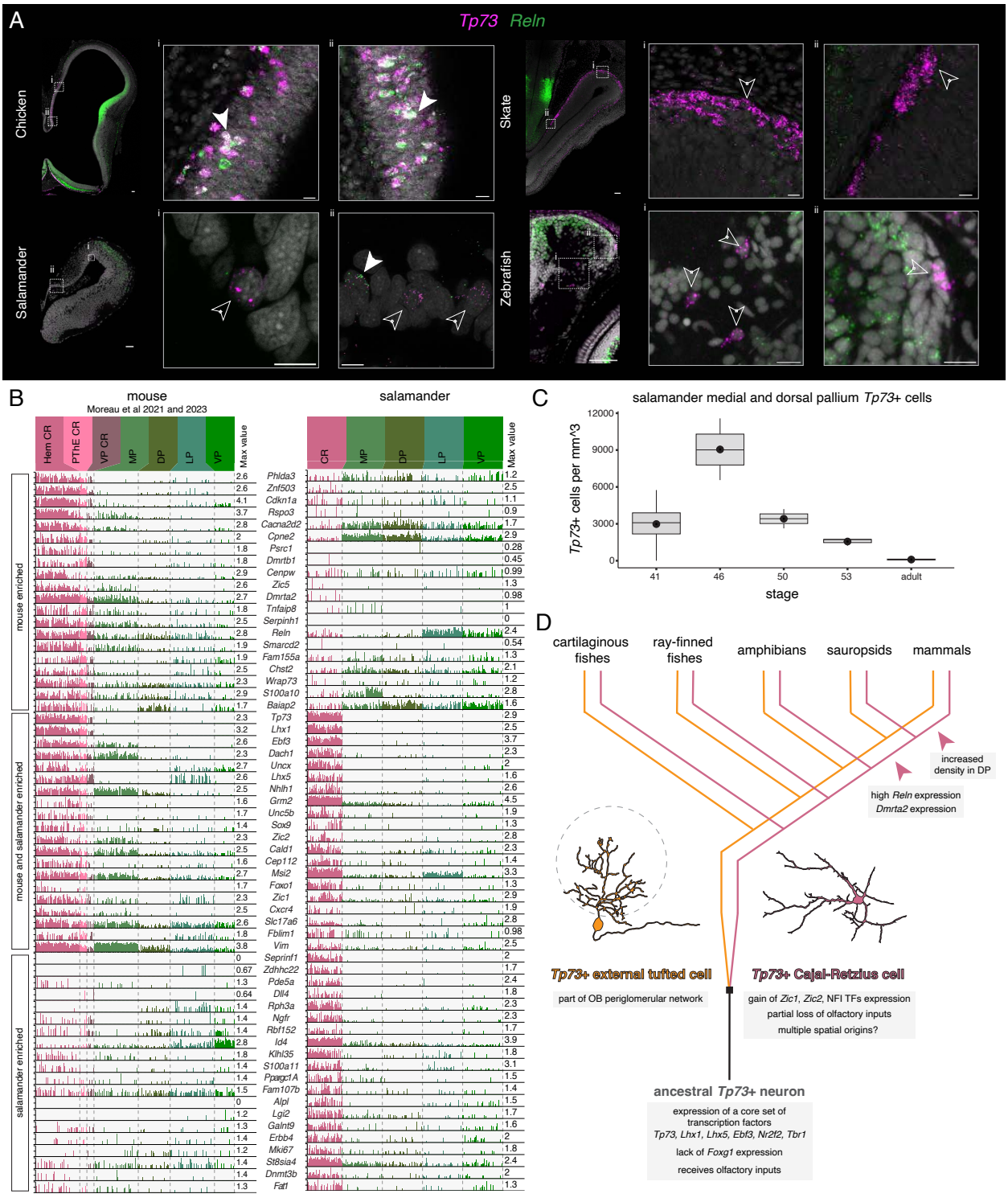

Figure 6. Transcriptomic divergence of vertebrate CR cells.
(A) HCRs showing *Reln* (green) and *Tp73* (magenta) expression on coronal sections of developing stage E6 chick, st.50 salamander and 6 dpf zebrafish brains, and an horizontal section of a stage 29 skate brain. Closed arrowheads indicate examples of *Tp73*+ *Reln*+ cells. Open arrowheads indicate examples of *Tp73*+ *Reln*-negative cells.

905 Scale bar 50um (Coronal Section) 10 um (Zoom Panel). (B) Expression of marker
906 genes that differentiate CR cells from other pallial glutamatergic neurons (ETCs
907 excluded) in mouse and salamander developmental datasets. The plot shows the top 20
908 genes enriched in mouse but not salamander CR cells; the top 20 genes enriched in
909 both species, and the top 20 enriched in salamander but not mouse CR cells (see
910 Methods). Mouse data from Moreau et al 2021 and Moreau et al 2023 [29,33]. (C)
911 Quantification of the density of *Tp73*+ cells in salamander medial and dorsal pallium
912 across developmental stages. Black dot represents average value. n= 3 animals for
913 stages 36-50 and adult, n=2 for stage 53. (D) Proposed evolutionary relationship
914 between CR cells and ETCs. Vertebrate phylogenetic tree with cell type typogenetic
915 tree superimposed (inspired by[74]). Schematics of ETC and CR cells (dorsal view) based
916 on[75,76]. Dotted circle represents OB glomerulus.
917 Abbreviations: DP, dorsal pallium; LP, lateral pallium; MP, medial pallium; VP, ventral
918 pallium
919
920

921

Materials and Methods

Animals

Salamander: *Pleurodeles waltl* adults and larvae were obtained from a breeding colony established at Columbia University. Animals were maintained in an aquatics facility at 20°C under a 12L:12D cycle. All experiments were conducted in accordance with the NIH guidelines and with the approval of the Columbia University Institutional Animal Care and Use Committee (IACUC). Breeding was induced naturally by manipulating water level and temperature. Experiments were performed with adult (5-19 months) male and female salamanders, and stage 30, 33, 36, 41, 46, 50, 53, and 55 embryos and larvae, staged according to the Gallien and Durocher 1957 [77] staging criteria. Embryos and larvae were anesthetized by immersion in a solution of 0.04% MS-222 (tricaine) for 5 minutes, while for adults a solution of 0.2% MS-222 in tank water was used. For stages 30-46, the brain was extracted directly after anesthesia, while stage 50-55 larvae were first perfused transcardially with 2 ml ice-cold PBS and adults with 10 ml ice-cold PBS and 10 ml of 4% PFA in PBS and decapitated before brain extraction. After overnight incubation in 4% PFA in PBS at 4C, brains were progressively dehydrated to 100% MeOH and stored at -20C.

Bichir fish: Adult *Polypterus senegalus* (~10 cm long) were purchased from commercial suppliers and kept in aquaria at Columbia University at 27C under a 12L:12D light cycle. All experiments were conducted in accordance with the NIH guidelines and with the approval of the Columbia University Institutional Animal Care and Use Committee (IACUC). Individuals were anesthetized using 0.4% MS-222 in tank water and then perfused transcardially with 20 ml ice-cold PBS and 10 ml ice-cold 4% PFA in PBS. After decapitation, the brain was extracted and fixed overnight in 4% PFA in PBS at 4C and dehydrated to 100% MeOH for storage at -20C.

Chicken: Fertilized eggs of White Leghorn Chicken (*Gallus gallus*) (Charles River) were incubated in a humidified chamber at 38°C, and embryos were staged according to[78]. Brains were dissected in cold PBS from embryos at E6, E8 and E16 stages. E16 embryos were perfused transcardially with 10ml cold PBS before dissection. Brains were immediately fixed overnight in 4% PFA in PBS at 4C, then dehydrated to 100% MeOH and stored at -20C.

Zebrafish: All zebrafish experiments were performed in accordance with the applicable regulations and approved by the Institutional Animal Care and Use Committee (IACUC) at Columbia University (protocol numbers AC-AABN3554 and AC-AACB9700). Wild-type AB zebrafish embryos at 2dpf and 3dpf, larvae at 6dpf and 15dpf, juvenile 45dpf juvenile, and adults of 3mpf and 6mpf were used. 2dpf and 3dpf (treated with PTU for depigmentation) embryos as well as whole 6dpf and 15dpf larvae were fixed overnight in 4% PFA. Additionally, whole brains from 6dpf, 15dpf, 45dpf, 3mpf and 6mpf zebrafish were also dissected after euthanization, and fixed in 4% PFA for overnight at 4°C. After fixation, next day samples were washed several times with PBS, then subjected to dehydration step by series of incubation in 25% MetOH - 75% PBS, 50% MetOH - 50% PBS and 75% MetOH - 25% PBS solutions for 10 minutes each, and finally transferred to 100% MetOH for storage at -20°C.

968 *Skate*: Little skate (*Leucoraja erinacea*) embryos were obtained from the Marine
969 Resources Center at the Marine Biological Laboratory (MBL) in Woods Hole, MA, USA.
970 All skate experiments were conducted according to protocols approved by the
971 Institutional Animal Care and Use Committee of the MBL. Embryos were reared to
972 stages S27, S29, S32 and hatchling stage as described in Gillis et al [79]. Embryos were
973 euthanized with an overdose of MS-222 (1 g/L in seawater), fixed overnight in 4% PFA
974 in PBS and stored in 100% MeOH at -20C. Hatchlings were anesthetized by immersion
975 in 0.5% MS-222 for 30 min, then perfused transcardially with 20 ml cold PBS and 10 ml
976 of 4% PFA in PBS. After decapitation, and brain extraction, brain tissue was fixed
977 overnight in 4% PFA in PBS at 4C and dehydrated to 100% MeOH for storage at -20C.
978
979 **Analysis of scRNA-seq datasets**
980 Selection of mature neurons from the developmental salamander dataset.
981 To analyze salamander neurons and compare them with neurons from other
982 species, we subsetted the full developmental dataset to include only mature neurons.
983 This selection allowed us to include data spanning multiple developmental stages where
984 we expected CR cells to be present, while preventing neuronal maturation from being
985 the dominant feature driving gene selection and downstream analyses.
986 Mature neurons from the full larval salamander data set (Deryckere et al 2025) [40] were
987 identified using the AddModuleScore_UCell function within the UCell package [80], and
988 using the following signature: positive genes: *Snap25, Syp, Stx1a, Mapt, Eno2, Map2*,
989 and negative genes: *Pcna* and *Mki67*. Cells were annotated as mature neurons if they
990 had a module score above 0.4. Mature neurons were only kept from clusters that
991 contained at least ⅔ mature neurons. This was done to remove sparse cells that had a
992 positive neuronal signature but were in primarily non-neuronal clusters. In order to
993 ensure all mature *Tp73*+ neurons were present for integration, special care was given to
994 these cells when identifying mature neurons. For any cell that was in the *Tp73*
995 subsetted object (see below), only cells in cluster clusters im1 and im2 were excluded
996 from the full mature neuron object.
997 Clusters were annotated by brain region (telencephalon, diencephalon, and midbrain)
998 based on marker genes curated from literature. Clusters were categorized as
999 Glutamatergic, Gabaergic or Other based on the expression of *Slc17a6*, *Slc17a7*, *Gad2*
1000 and *Th*.
1001
1002 Selection of mature neurons from the developmental mouse dataset.
1003 All cells published in the developing mouse brain atlas (La Manno 2021) [41] were
1004 filtered to remove cells with less than 2000 UMIs and with a percentage of mitochondrial
1005 genes above 10%. Cells annotated as “Hindbrain” were then removed because
1006 hindbrain cells were not included in the salamander and zebrafish datasets. Cells
1007 annotated by La Manno et al. as “Bad cells” were also removed. The remaining dataset
1008 was normalized using the Seurat SCTransform function while regressing for percent.mt,
1009 nCount_RNA, Age, and CellCycle. Clusters were computed using the Seurat
1010 FindClusters function with the parameters dims=35 and res = 8. Individual neurons were
1011 determined to be mature based on receiving a class annotation as “Neuron” from
1012 Lamanno et al. Clusters that contained at least ⅔ mature neurons were kept for further
1013 analysis. Regional identity of a neuronal cluster was established using marker genes

curated from literature. Clusters were categorized as Glutamatergic, Gabaergic or Other based on the expression of *Slc17a6*, *Slc17a7*, *Gad2* and *Th*.

Selection of mature neurons from the developmental zebrafish dataset.

The published scRNA-seq atlas from the developing zebrafish brain by Pandley et al was filtered to keep mature neurons according to their annotated clusters. First, all cells sampled from adult stages were removed, leaving 6 and 15dpf samples. Olfactory bulb neurons were kept as OB. Subpallium_01 to Subpallium_08 clusters were re-annotated as Telen GABA. Pallium_01 to Pallium_08 clusters were re-annotated as Telen Glut. Pallium_09 was re-annotated as Diencephalon based on the expression of *lhx1a*, *tbr1b*, *barhl2*, and lack of *tac3b* expression, which uniquely correlates with PThE based on results in MapZeBrain.org [81]. Preoptic area (PoA) and Habenula clusters were also annotated as Diencephalon. These subsetted neurons were normalized using the Seurat SCTransform function while regressing for stage. The top 3000 variable genes were used for downstream analysis, and the first 35 PCs were used for UMAP embedding.

Salamander *Tp73*+ neurons dataset

The Salamander *Tp73*+ neurons dataset includes cells selected from two datasets:

(1) From the developmental salamander brain dataset (Deryckere et al)[40]: clusters were computed from the full salamander developing brain object using the FindClusters function in Seurat with the res parameter set to 4. Clusters where *Tp73* was expressed in more than 5% of cells, and where the average scaled expression of *Tp73* was above 0.1 were selected for further analysis.

(2) From the adult salamander forebrain dataset (Woych 2022)[46]: two *Tp73*+ clusters (TEGLU31 and DIMEGLU6) were selected after the application of the same filtering criteria described above.

These selected developmental and adult *Tp73*+ clusters were then merged, reclustered and further filtered to keep only *Tp73*+ neurons, by removing choroid plexus, epithelial cells, progenitors, and some *Tp73*-negative neurons that made it through the previous round of filtering (details of filtering in code, and fig. S6). These final subsetted 982 *Tp73*+ neurons were normalized using the Seurat SCTransform function. The top 1000 variable genes that were expressed in at least 2.5% of cells were used for downstream analysis, and the first 20 PCs were used for clustering and UMAP embedding, with clusters calculated using a resolution of 1.55.

Mouse *Trp73*+ neurons dataset

Trp73+ forebrain neurons were identified from the full Allen Brain Cell atlas (Yao 2023)[39] based on the expression of *Trp73* and their annotation as neurons (*Trp73* is also expressed in some non-neuronal cell types). Groups were selected regardless of their level in the taxonomy. The final selection included: subclass 118 ADP-MPO Trp73 and cluster 2111 LHA Barhl2 Glut_2 (grouped as PV), supertype 0132 OB Eomes Ms4a15 Glut_3 (external tufted cells), and subclass HPF CR Glut (labeled as CR). Raw count matrices and metadata were downloaded from the Allen Brain Cell atlas portal in March 2024. These data are organized by dissected regions. Therefore each raw data

matrix was filtered to keep only cells belonging to the selected *Tp73*+ groups, and cells sequenced with the 10x v3 chemistry. This produced a final dataset of 2839 cells. This dataset was then normalized using the Seurat NormalizeData function, and the top 3000 variable genes were computed for downstream analysis.

Calculation of Gene Specificity Index (GSI) correlations.

GSI correlations between cell classes defined by region and primary neurotransmitter (see above) were computed using the method established in Tosches et al 2018. For the salamander-mouse comparison, differentially expressed genes were identified after running the Seurat FindAllMarkers function, using a 0.75 logfc.threshold and an adjusted p-value of 0.01. One-to-one orthologs were identified as described in Woych et al 2022 [46]. For the zebrafish-salamander comparison, differentially expressed genes were identified based on a 1 logfc.threshold and adjusted p-value of .001. Because teleost ancestors underwent a whole-genome duplication and zebrafish have several recently duplicated paralogs of tetrapod genes, an alternative to the standard one-to-one orthologue filtering was implemented. Eggnog [82] was run using taxonomic scope = vertebrates, Orthology restrictions = Any. For zebrafish genes that were orthologous to multiple different vertebrate gene names, only the one with the lowest e-value was kept. For multiple zebrafish genes that mapped to the same vertebrate gene name, the counts were summed and the vertebrate gene name was assigned for cross species comparison.

Marker gene enrichment analysis

To determine CR cell marker genes, CR cells were compared to other mature neurons (see above) in the La Manno et al. [41]. This list was filtered to keep genes that had an avg_log2FC >2 and a difference in percent of cells expressing the gene greater than .2 between the CR cells and other neurons. This list was then brought into salamander gene naming convention as described above. Orthologous genes were kept for module score calculation in salamander if they showed expression in the Seurat object (*i.e.* were listed as a feature). This final list of 49 marker genes was used as input to Seurat's AddModuleScore function. For the zebrafish analysis, the top marker genes for salamander *Tp73*+ neurons were computed using the same approach, yielding 42 marker genes.

Cross-species scRNA-seq integration

For cross species integration, genes between species were brought into the same naming convention as described above. Mature neurons from developing salamander, mouse and zebrafish were identified as described above, and further subsetted to include only forebrain neurons in the case of salamander and mouse. For Seurat CCA integration of mature neurons, we used functions within Seurat as follows: We selected 2000 integration features using "SelectIntegrationFeatures", and then subsetted this list for genes that were variable (based on variable.features.n = 4000) and expressed in at least 0.25% of cells in both species separately. The resulting list of integration features was passed to PrepSCTIntegration(). Then pairs of mutual nearest neighbors (anchors) were identified using the FindIntegrationAnchors function with the arguments reduction="cca" (Canonical Correlation Analysis) and normalization.method

1106 = SCT, before ultimately performing integrations using IntegrateData with 90 dims (in
1107 the case case of mouse to salamander) and 80 dims (in the case of salamander and
1108 zebrafish). The same dimensions used for integration were used for UMAP embedding.
1109 Clusters were calculated for the mouse-salamander integration using a clustering
1110 resolution of 1. Clusters were calculated for the salamander-zebrafish integration using
1111 a resolution of 2.
1112 The same pipeline was used for integration of *Tp73*+ neurons with the following
1113 exceptions: Initial identification of variable genes used a threshold of 8000 for each
1114 species, that needed to be expressed in 1% of cells within each original species (for
1115 zebrafish mouse integration, at least .1% of zebrafish cells to account for difference in
1116 sequencing depth), which was used to filter a list of 5000 integration features. 50
1117 dimensions were used for integration and UMAP embedding, and clustering was
1118 performed using a 0.1 clustering resolution for chicken and salamander with mouse,
1119 and .05 for zebrafish with mouse.
1120 As an alternative to co-clustering analysis, we analyzed cell type neighborhoods
1121 in the shared nearest-neighbor (SNN) graph computed by Seurat after integration. The
1122 SNN graph is the output of the FindNeighbors function and the input used for clustering.
1123 For each species and cell type, we counted the number of neighbors from the other
1124 species in the integrated SNN graph, and classified them according to cell type identity.
1125 This produced two matrices (*i.e.* salamander neighbors of mouse cells, and mouse
1126 neighbors of salamander cells) that were normalized by the total number of neighbors
1127 per source cell type, and then averaged to obtain the SNN proximity score.
1128
1129 Identification of differentially expressed genes between mouse *Tp73*+ neuron types
1130 Identification of marker genes for mouse *Tp73*+ CR and ETC cells were
1131 determined relative to *Tp73*-negative mitral and tufted cells (MT), which were the
1132 remaining supertypes in the 03-OB-CR Glut cell class in the Allen Brain Cell atlas.
1133 These MT supertypes were added to the mouse *Tp73*+ neurons object (described
1134 above), to generate a new object with 3516 cells, and were normalized using the Seurat
1135 SCTransform function. The top 3000 variable genes were used for downstream
1136 analysis. Marker genes were identified using the FindMarkers function within Seurat.
1137 Genes were listed as upregulated in either CR or ETC if relative to MT cells, they:
1138 had avg_log2FC>.5, had over a difference over 25% in the percentage of cells
1139 expressing the gene (*i.e.* 36% in CR, 10% in MT), had at least twice the percentage
1140 expressing the gene (*i.e.* 81% in CR, 40% in MT), and the differential expression of the
1141 gene received a p-value below 0.001. Genes were considered shared between CR and
1142 ETC if they were upregulated (relative to MT) in both lists. Genes were considered
1143 specific for CR or ETC if they were upregulated for one cell type but not the other, and
1144 were lowly expressed in the other cell type (below 25% of cells expressing the gene).
1145 Genes were filtered for display in Violin plots based on GO term. In order to show the
1146 conservation of gene expression across species, transcription factors that were
1147 expressed in both mouse CR and ETC had their expression checked in chick [54],
1148 salamander [40,46] and zebrafish [44]. TFs were included in Figure 4G if they were
1149 expressed in at least 2 species.
1150 For genes that differentially label CR cells from ETCs, Seurat FindMarkers was
1151 run to compare CR cells against ETCs in both the salamander and mouse data with

test.use="wilcox". Transcription factors that had over 25% difference in percent expression, an Avglog2FC above 2, below 35% expression in ETCs, and an adjusted p.value below .05 were considered CR specific markers for a species. The intersection of CR specific TFs between salamander and mouse is shown in figure 4. The same analysis was run to identify ETC specific markers across species but no transcription factors met the above significance threshold in both salamander and mouse.

Identification of differentially expressed CR markers between mouse and salamander

Comparisons of mouse and salamander CR marker genes were performed after computing differentially expressed genes between CR cells and other glutamatergic pallial neurons in developmental datasets. We filtered our data to ensure that the only *Tp73*+ cells were CR cells because we did not want to identify markers that are unique to basal forebrain or ETC *Tp73*+ neurons. In salamander, the *Tp73*+ neuron object was filtered to remove adult cells, as well as cells in clusters im1 and im2. Then, based on the *Tp73* integration described above, cells that clustered with mouse CR cells were labeled as salamander CR. This included all of m1.1 as well as a portion of m1.2. These 87 salamander CR cells were merged with 100 randomly selected mature neurons from each of MP, DP, LP and VP to create an object with 487 total cells. To obtain high quality developmental CR cells in mice we relied on published data from Moreau et al 2021 [33] for CR cells originating from hem, PThE, septum and ventral pallium, as well as Moreau et al 2023 [29] for hem-derived CR cells. All cells labeled as CR in Moreau et al 2021 were taken for further analysis as well as all clusters that could be annotated as dorsal, lateral or ventral pallium based on marker genes provided in their results. Data from Moreau 2023 were subsetted to only include CR cells and Pallial neurons, which in this case based on dissection and marker genes were all medial pallium. These cells were normalized using the SCTransform function while regressing for RNA count. The top 3000 variable genes were used for downstream analysis, and the first 50 PCs were used for clustering analysis and UMAP embedding; Louvain clustering was performed with a clustering resolution of 2. A random sample of 100 cells each was taken from the most mature cluster of Cell.state Cajal_retzius_neurons_LN and Pallial_neurons_LN based on the value of LN_signature1. Combining these cells with the subset from Moreau et al 2021 resulted in an object with 449 cells.

We then found differentially expressed genes between *Tp73*+ CR cells and Pallial glutamatergic neurons using the FindMarkers function with min.pct = .0001, logfc.threshold= .001, and test.use="wilcox". We labeled a gene as a CR marker if it had an average log-fold-change greater than 1 in CR cells relative to pallial neurons. We also filtered by adjusted p-value, only accepting DE genes with an adjusted p-value below 0.000001. Genes were categorized as species enriched CR genes if they appeared in the list of CR upregulated genes for their species but not in the list for the other, and the other species had below 33% expression of that gene in their CR cells. Genes were categorized as shared if they were in the list of upregulated CR genes for both species. For the plot in Figure 5A, the top 20 genes of each category were selected based on order of average log-fold change relative to the other pallial neurons. It is important to note that due to the selection of pallial glutamatergic neurons as the term of comparison, some known CR marker genes (such as the NFI TFs) were absent from the list, due to their widespread expression in medial and dorsal pallium.

1198 **Hybridization chain reaction (HCR) in situ hybridizations**
1199 Whole-mount HCR
1200 Whole mount HCR (hybridization chain reaction[83] in situ hybridizations were
1201 conducted as previously described in [46,84]. Briefly, whole brains of salamander embryos,
1202 larvae and adults, chicken E6 and E8 embryos, zebrafish 15-day larvae, and *Polypterus*
1203 adults, as well as whole skate S27 and S29 embryos were delipidated with overnight
1204 incubation in 100% Dichloromethane (DCM, Sigma-Aldrich 34856) and bleached
1205 overnight with 5% hydrogen peroxide in MeOH. Chicken, *Polypterus* and skate
1206 specimens were further incubated in bleaching solution (5% Deionized formamide, 1.5%
1207 H2O2, 0.2× SSC in nuclease-free water) for 40 mins under strong light. HCR-3.0 probe
1208 pairs were designed using **insitu_probe_generator** [85] and synthesized by Integrated
1209 DNA Technologies (IDT). Probes were added to Hybridization Buffer (Molecular
1210 Instruments) to a concentration of 12nM and incubated for three days at 37C. Samples
1211 were washed in Wash Buffer (Molecular Instruments) and SSCT (5xSSC + 0.1%
1212 TritonX) before incubation with 60pM snap-cooled HCR hairpins (Molecular
1213 Instruments) in Amplification Buffer (Molecular Instruments) for 3 days at 4C. Nuclear
1214 staining (DAPI or BOBO-1) was also added to the solution with a 1:1000 dilution. After
1215 washes in SSCT and 500 mM Tris-HCl (pH 7.0), samples were embedded in 4%
1216 agarose in 500 mM Tris-HCl (pH 7.0) and dehydrated to 100% MeOH overnight, then
1217 incubated with 66% DCM - 33% MeOH for 3 hours, 100% DCM for 30 min and 100%
1218 Dibenzyl ether (DBE, Sigma-Aldrich 108014) overnight. Cleared whole-brain samples
1219 were imaged using a LaVision UltraMicroscope II light-sheet microscope.

1220 After staining and agarose embedding, some whole-mount brains and all skate embryos
1221 were embedded in 4% agarose prepared in 500 mM Tris-HCl (pH 7.0), and then
1222 sectioned at 70 µm using a vibratome. Sections were incubated in DAPI diluted in Tris-
1223 HCl for 30 minutes, then mounted in either Fluoromount-G® (SouthernBiotech) or
1224 DAKO fluorescent mounting medium (Agilent Technologies) and imaged with a Zeiss
1225 LSM800 laser scanning confocal microscope.

1226 HCR on vibratome sections
1227 Brains of E16 chicken embryos and of skate hatchlings, and whole-mount 6-day
1228 old zebrafish larvae and S32 skate embryos were processed for HCR on sections.
1229 Brains stored in 100% MeOH were gradually rehydrated to PBS, then embedded in 4%
1230 agarose in PBS and sectioned using a Leica VT1200S vibratome. 100 µm thick sections
1231 of skate hatchling brain and 150 µm thick sections of chick E16 brains were then
1232 processed for HCR following[86]. Sections were first treated with bleaching solution (5%
1233 Deionized formamide, 1.5% H2O2, 0.2× SSC in nuclease-free water) for 30min under
1234 strong light, then rinsed in PBS and permeabilized for 1h with a solution of 1% Triton-X
1235 and 1% DMSO in PBS. After rinsing in SSCT sections were pre-hybridized in
1236 Hybridization Buffer (Molecular Instruments) for 1.5h at 37C and then incubated
1237 overnight with probes at 12nM concentration in Hybridization Buffer at 37C. The
1238 following day, samples were washed in Wash Buffer (Molecular Instruments) and then
1239 in SSCT, then incubated in Amplification Buffer (Molecular Instruments) for 30 min.
1240 Sections were then incubated overnight in the dark at RT with snap-cooled HCR
1241 hairpins (Molecular Instruments) at a concentration of 0.3µM in Amplification Buffer.
1242 Samples were rinsed several times with SSCT, mounted on glass slides with

1243 Fluoromount-G (Invitrogen, 00-4958-02) and imaged with a Zeiss LSM800 laser
1244 scanning confocal microscope.
1245
1246 Quantification of medial and dorsal pallium *Tp73*+ neurons during salamander
1247 development
1248 Coronal sections of pallium across developmental stages were stained and
1249 imaged as described above, using the 546 channel for *Reln* and the 647 channel for
1250 *Tp73*. Dense *Reln* expression in lateral pallium was used to delineate the boundary
1251 between dorsal pallium and lateral pallium. In posterior sections of the telencephalon
1252 the ventral boundary of the medial pallium was recognized from the clear separation of
1253 the pallium from septum. In more anterior sections, this boundary was recognized from
1254 a discontinuity of cell density between medial pallium and septum. For each coronal
1255 section, medial and dorsal pallium *Tp73*+ cells were manually counted across the Z
1256 width (with a z step of 3 um), and a *Tp73* density was calculated per section. These
1257 density data were then averaged for each brain to generate the plot in 5B.
1258
1259